NATIONAL ADVISORY COMMITTEE FOR AERONAUTICS

TECHNICAL NOTE 4005

AN EXPERIMENTAL INVESTIGATION OF THE EFFECT OF VARIOUS PARAMETERS INCLUDING TIP MACH NUMBER ON THE FLUTTER OF SOME MODEL HELICOPTER ROTOR BLADES

By George W. Brooks and John E. Baker

Langley Aeronautical Laboratory
Langley Field, Va.

Washington
September 1958

NATIONAL ADVISORY COMMITTEE FOR AERONAUTICS

TECHNICAL NOTE 4005

AN EXPERIMENTAL INVESTIGATION OF THE EFFECT OF VARIOUS PARAMETERS INCLUDING TIP MACH NUMBER ON THE FLUTTER OF SOME MODEL HELICOPTER ROTOR BLADES[1]

By George W. Brooks and John E. Baker

SUMMARY

Experimental studies were made to evaluate some of the effects of parameters such as Mach number, blade angle, and structural damping on the flutter of model helicopter rotor blades in the hovering condition. The model blades had NACA 23012 and 23018 airfoil sections and each was tested at chordwise center-of-gravity locations of approximately 27.5 and 37 percent chord. Data were obtained at test-medium densities ranging from 0.0012 to 0.0030 slug per cubic foot and at various pitch angles up into the stall. Mixtures of air and Freon-12 were used for the test medium in order to extend the tip Mach number range of the tests to slightly above unity.

Forward movement of the blade chordwise center-of-gravity location generally raised the flutter speeds at low pitch angles but had no appreciable effect at high pitch angles. An increase in the structural damping generally raised the flutter speed at high pitch angles. At a given pitch angle, the flutter occurred at essentially constant dynamic pressure for variations in density. A large beneficial effect of Mach number was observed near the section critical Mach number and was such that if flutter did not occur up to a tip Mach number of 0.73, it would not occur at all. Out of these studies a criterion is tentatively advanced which indicates design requirements for completely flutter-free operation of helicopter blades.

The significant flutter data for a large number of tests along with detailed descriptions of the models are included in tabular form to facilitate more detailed analyses of the results presented.

INTRODUCTION

The possibility of rotor-blade flutter exists for some helicopters of current and future types which are designed to operate at high tip

[1]Supersedes declassified NACA Research Memorandum L53D24 by George W. Brooks and John E. Baker, 1953.

speeds without being completely mass balanced about the blade 1/4 chord at all spanwise positions (ref. 1). Although the general characteristics of the flutter of propeller blades and wings in subsonic compressible flows at pitch angles up to and including the stall region have been studied by several investigators (e.g., refs. 2 and 3), no studies of similar nature have been reported in regard to helicopter blades. Theoretical methods are available which may be used to estimate the classical flutter speeds of helicopter blades in incompressible flows (refs. 4 and 5), but as yet neither theoretical nor experimental data have been presented for the prediction of the effects of compressibility or blade stall. In consideration of the differences between helicopter and propeller blades as to rigidity, structural damping, radius-to-chord ratio, solidity, root fixity, airfoil section, and so forth, some doubt exists as to the applicability of wing or propeller-blade flutter data to the prediction of the flutter characteristics of helicopter blades.

As a part of a general investigation of helicopter flutter, the present program was initiated in an effort to determine the effects of various parameters including Mach number, structural damping, and chordwise center-of-gravity location on flutter of model helicopter blades at zero forward velocity. The models had flapping hinges and plan forms representative of full-scale helicopter blades.

A portion of this investigation is devoted to the definition of a stall-flutter criterion for the design of helicopter blades which can be operated flutter-free throughout the pitch-angle range at all subsonic blade tip Mach numbers. Inasmuch as blade twisting deformations affect the blade pitch angle at flutter, and since the subject of blade twist may be of some general interest, a brief study of blade twist including the effects of Mach number is included.

SYMBOLS

a	slope of lift curve, $dc_l/d\alpha$
b	blade half-chord, ft
c	speed of sound in testing medium, ft/sec
c_l	section lift coefficient
$\overline{c_l}$	mean section lift coefficient
EI	blade bending stiffness, lb-in.^{2}
GJ	blade torsional stiffness, lb-in.^{2}

g_{h_1}	structural damping coefficient for first elastic bending mode
g_{h_2}	structural damping coefficient for second elastic bending mode
g_α	structural damping coefficient for first torsion mode
I_α	blade mass moment of inertia about elastic axis, slug-ft^2/ft
I_1	mass moment of inertia of blade including blade shank about flapping hinge, slug-ft^2
I_r	mass moment of inertia of blade shank about flapping hinge, slug-ft^2
m	blade mass per unit length, slugs/ft
m_r	mass of blade shank, slugs
M	rotational Mach number
q	dynamic pressure, lb/sq ft
r_α^2	nondimensional radius of gyration of blade section about elastic axis, I_α/mb^2
R	rotor radius, ft
V	section speed, fps
x_{cg}	section center-of-gravity location, percent chord
x_{EA}	section elastic-axis location, percent chord
α	angle of attack, deg
γ	mass constant of rotor blade, $2b\rho aR^4/I_1$
$1/\kappa$	blade mass-density ratio, $m/\pi\rho b^2$
θ	blade pitch angle between chord line and plane of rotation, deg
$\Delta\theta$	measured blade twist, deg

ρ density of testing medium, slugs/cu ft

σ rotor solidity, $2b/\pi R$

ω_f flutter frequency, radians/sec

ω_{h_1} experimental nonrotating natural frequency for first elastic flapwise bending mode, radians/sec

ω_{h_2} experimental nonrotating natural frequency for second elastic flapwise bending mode, radians/sec

ω_α experimental nonrotating natural frequency for first torsion mode, radians/sec

Subscripts:

o standard atmosphere

0.8R 0.8 rotor radius

t blade tip

c corrected for aerodynamic and dynamic twist

s initial setting

cr critical value

Notation for test rotor blades:

(f) forward chordwise center-of-gravity location

(r) rearward chordwise center-of-gravity location

APPARATUS AND TEST METHODS

The experimental investigations of helicopter-rotor-blade flutter reported herein were conducted in the Langley vacuum sphere (ref. 2). This facility consists of a steel tank in which is mounted a 500 horsepower electric motor which is used to whirl the rotor assemblies. The sphere can be evacuated to provide different air densities; or it can be filled with Freon-12 gas, or mixtures of air and Freon-12, at various densities. The combined use of air and Freon-12 provides a means for studying independently the effects of Mach number and velocity on flutter.

Blade configuration.- The blades used in the tests were designed to be geometrically representative of normal helicopter configurations, and to flutter at speeds which would yield useful data at Mach numbers where compressibility effects might become important over a range of pitch angles and chordwise center-of-gravity locations. The blades were of composite wood construction with a stainless-steel rod (spar) embedded in the wood and extending longitudinally along the quarter-chord line. Three holes extending parallel to the main spar were routed in the blades, one at each of the following points: 6.25, 50, and 62.5 percent chord, as shown in figure 1. The chordwise center-of-gravity position was varied by means of selective location of stainless-steel rods or inserts in these holes. The structural damping of the blades was varied in some cases by wrapping these rods with cloth.

The blades studied had NACA 23012 sections with chordwise center-of-gravity locations of 27.5 and 37.3 percent chord, and NACA 23018 sections with chordwise center-of-gravity locations of 28.0 and 36.5 percent chord. The rotor assembly including the blade, blade shank, hub, and counterweights is shown in figure 2. The blades were tested as one-blade configurations and the active portion of the blade extended from a radius of 8 inches to a radius of 46 inches with a flapping hinge located at a radius of 2.5 inches. No drag hinges were used. The centrifugal forces were balanced by adjustable counterweights.

The blade dimensions, natural frequencies, and other pertinent flutter parameters are given in table I. The frequencies were measured with the blades mounted on the hub in the test condition, that is, free to flap. The blades are grouped according to airfoil section, blades 1 to 5 having NACA 23012 airfoil sections and blades 6 to 9 having NACA 23018 airfoil sections. During the tests, blade 2 was observed to have warped slightly, resulting in an upward deflection of the trailing edge. Models 1, 2, 3, and 4 were separate blades. Blade 5 was obtained by wrapping the rods of blade 4 with cloth to increase the structural damping. This also resulted in an increase in torsional stiffness. Models 6 and 7 were also separate blades. The rods of blade 7 were wrapped with cloth as previously mentioned. This modification resulted in a blade having two new values of the torsional structural damping coefficient; one value for low-amplitude vibrations and another for high-amplitude vibrations. These new configurations are referred to as blade 8 and blade 9, respectively. The blade numbers are accompanied by the letters (f) and (r) which are used to designate forward and rearward chordwise center-of-gravity locations, respectively.

Instrumentation and data observations.- Flutter data were obtained through the use of wire strain gages cemented to the blades in such a way as to indicate both torsional and bending deflections, figure 2. The strain-gage outputs together with a tachometer signal for measuring the rotational speed were recorded on oscillograph records such as shown

in figure 3. The end of the blade was illuminated instantaneously at a predetermined point in each revolution by means of a strobolight energized through a contactor on the motor shaft. The image of the blade tip, thus obtained, was used to measure the pitch angles at the blade tip by use of a telescope with the eyepiece graduated for angular measurements. The pitch-angle measurements were then used to determine the amount of blade twist for various test conditions.

Flutter testing procedure.- The blades were operated with the pitch angle fixed at the blade root. The pitch angle was changed between tests to obtain data over a range of pitch angles from about 8° to 30°. The operating procedure for each flutter test consisted of slowly increasing the speed of the test blade until strong flutter was first encountered, at which point an oscillograph record was taken. The pitch angle at the blade tip was then measured at a slightly lower speed (40 to 80 rpm lower) in order to have the blade in a more stable condition. The flutter region was often penetrated, in attempting to find an upper boundary, until either the flutter became too severe or the flutter region was traversed. In the latter case, a record was taken upon reentering the flutter region from the top.

The effect of Mach number on the flutter characteristics was studied by use of various mixtures of Freon-12 gas (sound speed approximately equal to 500 fps) and air at various densities ranging from 0.0012 to 0.0030 slug per cubic foot. The blades were initially fluttered in air at various densities after which they were tested in nearly pure Freon-12 gas. The percentage of Freon-12 was then lowered by steps, thus raising the sound speed of the mixture until the desired range of sound speed had been covered. Flutter data were obtained at various densities for each mixture by variation of the absolute pressure of the testing medium. As a result of the flutter tests being made in the aforementioned gaseous mediums over a relatively wide range of velocities, tip Mach numbers up to 1.1 could be reached, and the Reynolds number at the blade tip for the tests varied from about 125,000 to about 2,250,000.

RESULTS AND DISCUSSION

General Considerations

Flutter parameters and reference stations.- The flutter data are presented as functions of the flutter speed coefficient $V/b\omega_\alpha$, a design parameter $b\omega_\alpha/c$, the tip Mach number M_t, the density ratio ρ/ρ_o, and the pitch angle θ. In some instances, the data are also presented in terms of combinations of these parameters, for example, $\left(V/b\omega_\alpha\right)\sqrt{\rho/\rho_o}$.

The significance of these parameters in propeller-blade and wing stall flutter studies is recognized and discussed in some detail in references 2 and 3.

The flutter speed coefficient as well as the blade pitch angles and pitch-angle settings are referred to the station at 0.8R; however, the Mach number and measured blade twist are referred to the blade tip. These reference stations were chosen because (1) the velocity of the element at 0.8 blade radius appears to be more representative for flutter than the element at 0.75 radius which is usually referred to in helicopter analyses, (2) the tip Mach number readily identifies the Mach number at any radial location, and (3) the twist at the tip is the measured twist.

Lift coefficient.- In order to facilitate the estimation of the blade loading at flutter, figure 4 shows the mean section lift coefficient as a function of the pitch angle as calculated by means of reference 6 for an element located at the 0.8 blade radius assuming this station to be typical. Inasmuch as the lift curves for NACA 23012 and 23018 airfoil sections are not appreciably different, a mean value of the slope of the lift curve is assumed and a single mean-value curve of $\overline{c_l}$ plotted against θ is presented for the representation of both blades.

Presentation of Flutter Data

The significant parameters for the blades tested are given in table I and discussed in the previous section entitled apparatus and test methods. The detailed results of the flutter investigation are tabulated in table II, according to blade section, blade number, and chordwise center-of-gravity location. The general sequence of presentation corresponds closely to the order in which the data were taken.

Some of the general trends determined during the investigation are discussed in the following paragraphs with the aid of samples of data presented in figures 5 to 16. The presentation of the flutter results is divided into two parts: the first relating to data taken at Mach numbers where compressibility effects were found to be insignificant, and the second relating to the effects of Mach number and the effects of various flutter parameters at Mach numbers where compressibility effects appeared to be important.

In addition to the experimental flutter investigation, a limited study was made to determine blade twist as influenced by dynamic pressure, flutter and divergence, and Mach number. The results of this study are presented in the appendix and in table III and are discussed with the aid of figures 17 to 21.

Discussion of the Effects of Various Parameters on Flutter at Low Mach Numbers

Blade pitch angle.- The general shapes of the characteristic flutter curves obtained for propeller blades and wings in essentially incompressibile flows by plotting the flutter speed coefficient as a function of the blade pitch angle or angle of attack have been established by the work of several investigators (e.g., refs. 2 and 3). Figures 5 to 8 of this paper present some experimental results of a similar nature obtained for some model helicopter blades which show the characteristic shapes of the flutter curves as well as the effect of various flutter parameters.

The flutter data for a typical blade are shown in figure 5 where both the flutter speed coefficient and the ratio of the flutter frequency to blade first natural torsional frequency are plotted as a function of blade pitch angle. The curve of flutter speed coefficient, or flutter curve, separates the stable and unstable regions; the unstable region being above the flutter curve. As the blade pitch angle is increased, the flutter speed coefficient drops slightly at first and then rapidly as the blade apparently begins to stall. As the pitch angle is further increased, the flutter speed coefficient decreases until some minimum value is reached. Further increases in pitch angle result in a rather sharp rise in the flutter speed coefficient, possibly due to a rearward shift in center of pressure arising from blade stall. The curve of frequency ratio shows that a reduction in the value of the flutter speed coefficient is accompanied by an increase in flutter frequency.

The upper portion of the flutter curve, corresponding to low pitch angles, defines the region of classical flutter whereas the lower portion of the curve defines the region of stall flutter. Classical flutter usually involves a coupling of blade motion in at least two degrees of freedom. Since flutter occurs in the mode representing minimum potential, the significant modes for conventional helicopter blades are probably blade torsion and flapping. As shown by the frequency-ratio curve of figure 5, the classical flutter occurs at a frequency considerably lower than the first torsion natural frequency. Stall flutter on the other hand is a predominantly torsional oscillation, the frequency of which is shown by figure 5 to be very nearly equal to the first torsional natural frequency. Some flutter of the wake-excited type (see ref. 7) was also obtained. This flutter occurred at pitch-angle settings near 0°, at speeds of the order of 85 percent of the classical flutter speed, and at frequency ratios of the order of $\frac{\omega_f}{\omega_\alpha} = 0.80$.

Now that the characteristic shape of the flutter curve for a typical blade is established, the following paragraphs along with figures 6 to 9 will be devoted to an analysis of the effects of various flutter parameters. The absence of data at low pitch angles is due to the fact that the blades were designed so that the flutter speeds at high pitch angles would be sufficiently high to permit the evaluation of Mach number effects when the blades were tested in mixtures of air and Freon-12. Consequently, at low pitch angles, where the flutter speed is appreciably higher, the maximum operating speed was limited by centrifugal stresses rather than flutter.

Chordwise center-of-gravity location.- The effect of chordwise center-of-gravity location on the flutter speed coefficient as a function of blade pitch angle is shown in figure 6 for blades having both NACA 23012 and NACA 23018 airfoil sections. In each case, a rearward shift in chordwise center-of-gravity location lowers the flutter speed coefficient appreciably at the lower pitch angles but has little effect on the minimum values obtained at high pitch angles in the stall region; a similar effect was also obtained for some additional model tests wherein the chordwise center-of-gravity location was moved forward as far as 22.5 percent chord. This result is apparently at variance with the results of a similar investigation of propeller blades reported in reference 2 which showed the value of the minimum flutter speed coefficient to be very much a function of the chordwise center-of-gravity location. The relation of this difference in behavior to specific differences in propeller and helicopter blade stall characteristics is not clear at present.

Airfoil section.- During the investigation, it was observed that one of the blades had warped slightly, and this warping resulted in a slight upward deflection or reflection of the trailing edge. The curve of flutter speed coefficient as a function of blade pitch angle for this blade is presented with a similar curve for a blade without reflex trailing edge in figure 7. A comparison of the respective curves shows that, at pitch angles in the region of transition between classical and stall flutter, the flutter speed coefficient is considerably less for the blade having the reflex trailing edge than for the blade without the reflex trailing edge. The difference between the curves decreases, however, as the pitch angle increases and becomes nonexistent at stall. The earlier transition from classical flutter to stall flutter for the warped blade may be caused by the negative camber due to the warping. The data in reference 8 show that blades having less camber have lower flutter boundaries at pitch angles lower than the stall.

A comparison of the data presented in figures 8(a) and 8(b) shows that, at pitch angles of the order of 14°, the discrepancies between the flutter curves of the blades having different airfoil sections are small. As the pitch angle is increased, the flutter speed coefficients, for blades having similar torsional structural damping coefficients but different airfoil thickness, are considerably different. This appears to be due to the relative indifference of the minimum flutter speed

coefficient for the 18-percent-thick blades to variations in structural damping in the range of $g_\alpha = 0.06$.

Structural damping.- The most pronounced effect of structural damping at low Mach numbers occurred at blade pitch angles in the stall region. Figure 8(a) shows that, for blades having NACA 23012 airfoil sections, the minimum flutter speed coefficient is increased appreciably by raising the torsional structural damping coefficient from $g_\alpha = 0.049$ to 0.067. A variation in damping over a similar range ($g_\alpha = 0.054$ to 0.069), as shown in figure 8(b), did not appreciably affect the minimum flutter speed coefficient of the blades having NACA 23018 airfoil sections. However, when the structural damping coefficient for the NACA 23018 airfoil section was approximately tripled, a significant rise in the minimum flutter speed coefficient was obtained.

In addition to the effect of structural damping on the magnitude of the minimum flutter speed coefficient, it was observed that the flutter which occurred on the blades having high torsional structural damping coefficients was usually more violent than the flutter of the blades having low structural damping coefficients. This effect was more pronounced at the pitch-angle setting corresponding to the minimum flutter speed coefficient, and may be due to the coupled effects of nonlinearities in the structural and aerodynamic properties of the blades while operating in the flutter region.

Density.- Although the discussion presented in the previous sections was limited to data obtained at atmospheric density, data were also obtained at densities ranging from approximately 0.0012 to 0.0030 slug per cubic foot. Inasmuch as the flutter speeds obtained during the tests were found to be a function of the density, the question arose as to the most convenient method of presenting the data for different densities. An empirical expression for the classical flutter speed of a wing is given in reference 9 which shows the flutter speed to be inversely proportional to the square root of the density of the testing medium for wings having small values of the bending-to-torsion frequency ratio and values of $1/\kappa > 10$. Since the values of these parameters for the blades tested were well within the limits given in reference 9, there was reason to expect that, at low pitch angles in the region of classical flutter, the blades would flutter at constant dynamic pressure at a given pitch angle. This proved to be the case not only at low pitch angles but at high pitch angles as well. This is shown by the samples of data presented in figure 9 where the flutter speed coefficient is plotted as a function of the density ratio for medium and high pitch angles. Inasmuch as the straight lines through the data points show that $V_{0.8R}/b\omega_\alpha = C_1\sqrt{\rho_o/\rho}$, then by simple manipulation it can be shown that $\frac{1}{2}\rho V^2 = C_2$, where C_1 and C_2 are constants

which depend on the slope of the straight line and consequently are functions of the blade-pitch-angle setting. The high pitch-angle setting is near the stall angle, and the flow is probably of a non-potential nature at least during a portion of the flutter cycle.

The fact that the flutter at high pitch angles occurred at constant dynamic pressure rather than constant velocity is at variance with most of the experimental results previously obtained for wings and propellers, references 2 and 3. This difference may be due to the fact that the structural damping is much greater in the present case than for previous tests, or it might be due to aerodynamic differences associated with the different airfoil sections. The analytical and experimental investigation of reference 3 indicates that when the structural damping is very low, the minimum value of the flutter speed coefficient is essentially independent of density and the flutter will depend on the aerodynamic damping of torsional oscillations. The aerodynamic damping coefficients are shown in reference 3 to be a function of velocity and chordwise location of the torsional axis of rotation and independent of density. If, for a given axis of rotation, a region of negative damping exists, then the flutter velocity is equal to the velocity at which the aerodynamic damping becomes negative. However, if the structural damping is substantial, as is generally the case for helicopter blades, then the minimum flutter speed is shown in reference 3 to increase as the function $g_\alpha(r_\alpha^2/\kappa)$ increases. If $g_\alpha(r_\alpha^2/\kappa)$ be written in the equivalent form $g_\alpha(I_\alpha/\pi\rho b^4)$, then the minimum flutter speed is shown to increase as the density decreases, a condition which is borne out by the results of the present investigation. Whether a similar effect would be obtained by varying the mass moment of inertia I_α at constant density is uncertain since no tests of this nature were made.

Discussion of the Effects of Various Parameters on Flutter at High Tip Mach Numbers

The fact that the flutter at a given pitch angle occurred at constant dynamic pressure, as previously discussed, greatly simplifies the presentation of the data at higher Mach numbers. It effectively means that these data, taken at various densities and Mach numbers, can be represented by single curves for the different pitch-angle settings. The data presented in figure 10 for three ranges of density ratio show that the flutter boundaries obtained by plotting the flutter speed coefficient as a function of tip Mach number for various pitch-angle settings are not altered appreciably by changes in density when the flutter speed coefficient is modified by the square root of the density

ratio. This simplification is employed in subsequent discussion where the data taken at various densities are plotted in terms of the modified flutter speed coefficient $\left(V_{0.8R}/b\omega_\alpha\right)\sqrt{\rho/\rho_o}$.

Samples of the experimental data showing the effects of Mach number on the modified flutter speed coefficient at various blade pitch angles are shown in figures 11 and 12. These data are replotted in another form in figures 13 to 16 for use in establishing a design criterion. The operating line shown in figure 11(a) represents the line along which a given helicopter blade operates as the rotor speed is varied in a medium having a constant speed of sound. The slope of the operating line is inversely proportional to $b\omega_\alpha$ and directly proportional to the sound speed. Variation of any of these factors will result in an operating line having a different slope.

Blade pitch angle.- The trends of flutter speed coefficient with blade pitch angle at the lower Mach numbers as shown in figures 11 and 12 are the same as those presented in figures 5 to 8. As the Mach number is increased, for each pitch-angle setting lower than the angles for minimum flutter speed coefficients, a reduction is noted in the flutter speed coefficient until some Mach number of the order of magnitude of the tip-section critical Mach number is reached. Further increases in Mach number result in a rapid rise in the flutter speed coefficient.

Although the decrease in the flutter speed coefficient is in the direction associated with compressibility effects, blade twist arising from aerodynamic forces and centrifugal body forces may be a contributing factor. The data are not sufficient to permit a generalization at this time as to the magnitude or direction of twist effects. However, some effects of Mach number on blade twist are discussed in the appendix. The tendency for a reduction in flutter speed coefficient with increasing Mach number diminishes and essentially disappears at a pitch angle approximately equal to the angle for minimum flutter speed coefficient. The magnitude of the reduction in flutter speed coefficient with increasing Mach number appears to vary somewhat from blade to blade. This is shown by a comparison of figures 11(a) and 11(b) where similar data are presented for blades number 2(r) and 3(r), respectively. The primary difference between the blades is the structural damping coefficient for torsion (see table I); the damping coefficient of blade 3(r) being about half that of blade 2(r).

The turnback of the flutter curves for the various pitch-angle settings represents a beneficial Mach number effect which is very similar to that exhibited by propellers (ref. 2). This beneficial effect is possibly due to a rearward shift of the center of pressure. An envelope flutter boundary can be drawn which separates the flutter regions for all

pitch-angle settings from the flutter-free or stable regions as shown by the crosshatched curves of figures 11 and 12.

Airfoil thickness.- A comparison of figures 11(a) and 12(a) shows that the minimum flutter speed coefficient of the envelope flutter boundary for the 12-percent-thick blade is somewhat higher than that for the 18-percent-thick blade. In addition, the envelope flutter boundary for the 12-percent-thick blade turns back much more abruptly than that for the 18-percent-thick blade; however, the envelope flutter boundaries for both blades extend to a maximum Mach number of 0.73. In both cases the individual flutter boundaries, for some blade-pitch-angle settings and at Mach numbers above the Mach number at which the turnback occurs, do not tend to coincide with the respective envelope flutter boundaries but rise more steeply. This effect is noted for the 18-percent-thick blade at pitch-angle settings of 11.3°, 16.1°, and 20.1°, all of which are lower than the angle for minimum flutter speed coefficient. For the 12-percent-thick blade, the effect is evident at a pitch-angle setting of 21.7°, which is greater than the angle at which the minimum flutter speed coefficient occurs. In this case, the flutter boundary turns back before the envelope flutter boundary is reached. The existence of flutter boundaries which lie within the envelope flutter boundaries is a beneficial effect of Mach number over and above that exhibited by the envelope flutter boundaries themselves.

Section center-of-gravity location.- The effect of chordwise center-of-gravity location on the turnback of the flutter boundaries for different pitch-angle settings is shown for the 18-percent-thick blade by a comparison of figures 12(a) and 12(b). The data indicate that the turnback of the individual flutter boundaries for the higher pitch angles occurs at lower Mach numbers for the blade having the forward center-of-gravity location. This trend of the flutter boundaries indicates that an increase in Mach number results in a rearward shift of the center of pressure, the effect of which is apparently greater at high pitch angles. Inasmuch as the forward chordwise center-of-gravity location is near the quarter chord, (about 28.0 percent), only a slight rearward movement in center of pressure is necessary to alter appreciably the blade torsional moments, and therefore it appears logical that this effect would be more pronounced at the forward location of the center of gravity as indicated by the data. The flutter data for the 12-percent-thick blades do not indicate the same trend. It is possible that there is a smaller effect of Mach number on the location of the center of pressure for the thinner blade.

Design Criterion

A summary of the data presented herein indicates a possible design criterion that may be used to select helicopter blades which can be

operated flutter-free throughout the subsonic speed range. The nature and significance of this tentative criterion may be better understood by a discussion of the manner in which it is derived and of the blade parameters involved.

Maximum Mach number at flutter.- An analysis of the data presented in table II, a portion of which is plotted in figures 11 and 12, shows that the over-all Mach number effect was such that, for the blades tested, if flutter did not occur at a tip Mach number less than about 0.73, it would not occur at any tip Mach number up to a value slightly greater than unity, the limit of the tests. The fact that the flutter boundary occurs at a tip Mach number of about 0.73 may be associated with local supercritical flow conditions and to the rearward movement of the center of pressure which is a stabilizing condition. Some evidence of this is shown by the blade-twist data presented in the appendix.

Derivation of flutter parameters.- The operating line on a flutter plot of the type shown in figures 11 and 12 is a straight radial line from the origin, the slope of which is inversely proportional to the dimensionless flutter parameter $\left(b\omega_\alpha/c\right)\sqrt{\rho_o/\rho}$. A particular operating line is shown in figure 11(a). The extent to which a blade will be subjected to flutter as the rotor speed is increased depends on the slope of the operating line and the blade pitch angle. As the slope of the operating line is decreased, or conversely, as the flutter parameter $\left(b\omega_\alpha/c\right)\sqrt{\rho_o/\rho}$ is increased, the ranges of pitch angles and speeds wherein flutter may be obtained gradually decrease and disappear when the operating line becomes tangent to the envelope flutter boundary. Thus the flutter parameter $\left(b\omega_\alpha/c\right)\sqrt{\rho_o/\rho}$ is significant in flutter studies. Its magnitude may be varied by varying the blade chord, blade torsional frequency, or testing medium. Generally, values of the blade chord and torsional frequency are to some extent under the control of the designer. However, it is sometimes more convenient from a research standpoint to vary the testing medium as was done in the present investigation.

In order to demonstrate more clearly the effect of the flutter parameter $\left(b\omega_\alpha/c\right)\sqrt{\rho_o/\rho}$ on the flutter of the model blades, the data of figure 11(a) is first cross-plotted as shown in figure 13. This is accomplished by drawing a series of radial or operating lines from the origin of figure 11(a), each of which has a slope of constant $\left(b\omega_\alpha/c\right)\sqrt{\rho_o/\rho}$. Upon intersection of a particular radial line with the flutter curve for a given pitch-angle setting, the value of the tip Mach number is noted. The mean twist for the pitch-angle setting is then obtained from table II. Assuming a linear radial distribution of twist, the twist at 0.8R is

calculated and added algebraically to the pitch-angle setting to obtain the actual pitch angle at 0.8R at flutter. The Mach number at flutter is then plotted against the corrected pitch-angle setting $(\theta_{0.8R})_c$ for the various constant values of $(b\omega_\alpha/c)\sqrt{\rho_o/\rho}$ as shown in figure 13. The Mach number at flutter is then replotted as shown in figure 14 as a function of the flutter parameter $(b\omega_\alpha/c)\sqrt{\rho_o/\rho}$ for various pitch angles. The lower or envelope flutter boundary is simply a transformation of the envelope flutter boundary of figure 11(a).

Discussion of design criterion.- The presentation of the data in the form of figure 14 permits a more rational evaluation of the role of some of the parameters on the envelope flutter boundary, and facilitates the discussion of the flutter region in terms of the flutter parameter $(b\omega_\alpha/c)\sqrt{\rho_o/\rho}$. The figure shows that there is a maximum value of $(b\omega_\alpha/c)\sqrt{\rho_o/\rho}$ above which no flutter was obtained for tests up to a tip Mach number slightly greater than unity, and this value is termed the critical value. Thus a possible criterion for stall flutter is indicated. Since, for practical applications, the sound speed is a constant, it may be possible for blades having a value of $b\omega_\alpha$ greater than the value corresponding to this critical value to be operated flutter-free throughout the pitch-angle and Mach number range.

In order to facilitate a comparison of the results in terms of the flutter parameter for various blades having different thickness, chordwise center-of-gravity location, and structural damping, the data presented in table II were plotted and cross-plotted as discussed in the previous paragraphs to obtain envelope flutter boundaries similar to the one shown in figure 14. The resulting envelope flutter boundaries are shown in figure 15. The critical values of these envelope flutter boundaries are replotted in figure 16 as a function of structural damping. Data are also presented showing critical values of $(b\omega_\alpha/c)\sqrt{\rho_o/\rho}$ for the propeller of reference 2 and the wing of reference 3.

There are no apparent effects of chordwise center-of-gravity location or thickness on the critical values of $(b\omega_\alpha/c)\sqrt{\rho_o/\rho}$. There is, however, an upward trend of the critical values as the torsional damping is reduced, and, on the basis of these results, a design criterion can be stated, namely, that helicopter blades having values of structural damping above 0.03 should be able to operate completely flutter-free if the value of the design parameter $(b\omega_\alpha/c)\sqrt{\rho_o/\rho}$ is greater than 0.3.

The critical values of $(b\omega_\alpha/c)\sqrt{\rho_o/\rho}$ for the wing and propeller results as shown in figure 16 are appreciably higher than those for the helicopter blades tested, but the structural damping coefficients for the wing and propeller were much smaller than those for the helicopter blades. Structural damping appears to have considerable effect on the critical values of $(b\omega_\alpha/c)\sqrt{\rho_o/\rho}$, but no conclusion can be drawn comparing the propeller and wing flutter criterion to the helicopter-blade flutter criterion since the length-to-chord ratio as well as section thickness ratio for the helicopter blades were much higher than for the wing and propeller.

It should be emphasized that the results reported herein apply specifically to the hovering case and may not be valid for conditions of forward flight.

CONCLUSIONS

The results of an experimental flutter investigation conducted in the Langley vacuum sphere flutter test apparatus to determine the effects of various parameters including Mach number on the flutter of some model helicopter rotor blades indicates the following conclusions:

1. Forward movement of the chordwise center-of-gravity location raised the flutter speed coefficient at low pitch angles, but had relatively little effect on the flutter speed coefficient at high pitch angles.

2. The minimum values of the flutter speed coefficient increased with increases in the torsional structural damping coefficient.

3. At a given Mach number and blade-pitch-angle setting, flutter occurred at essentially constant dynamic pressure at densities ranging from 0.0012 to 0.0030 slug per cubic foot. This was observed at all pitch angles up to the angle corresponding to minimum flutter speed coefficient.

4. At blade pitch angles below the stall angle, the flutter speed coefficient decreased as the Mach number was increased up to a certain value of Mach number, above which the flutter speed coefficient increased rapidly. The initial reduction disappeared at pitch angles near the stall angle.

5. For the blades tested, if flutter did not occur at a tip Mach number less than 0.73, it would not occur at any tip Mach number up to slightly greater than 1, the limit of the tests.

6. A tentative design criterion based on the particular tests covered is presented. This criterion implies that helicopter blades having values of the torsional structural damping coefficient greater than 0.03 and the design flutter parameter $(b\omega_\alpha/c)\sqrt{\rho_o/\rho}$ above 0.3 should be able to operate completely flutter-free. (b = blade half-chord; ω_α = natural first torsional frequency; c = speed of sound in testing medium; ρ_o = standard density; and ρ = operating density.)

Langley Aeronautical Laboratory,
National Advisory Committee for Aeronautics,
Langley Field, Va., May 5, 1953.

APPENDIX

A BRIEF STUDY OF BLADE TWIST AS INFLUENCED BY BLADE PITCH ANGLE, DYNAMIC PRESSURE, FLUTTER AND DIVERGENCE, AND MACH NUMBER

Inasmuch as the flutter characteristics of the blades tested were found to be dependent on the blade pitch angle, it was of interest to obtain some over-all indication of the manner in which blade pitch angle was altered by blade twist. Perhaps of greater importance though is the fact that the blade twist is a good qualitative index of the chordwise location of the center of pressure, which appears to have considerable influence on the flutter characteristics of the blades. Figures 17 and 18 present some experimental measurements which show the blade twist, measured at the tip, for a 12-percent-thick blade with the chordwise center of gravity located at 37.3 percent chord. Figure 19 presents a comparison of experimental and calculated values of blade twist at a low pitch angle at rotor speeds approaching the blade divergence speed. Figures 20 and 21 show some experimental results, tabulated in table III, as to the effect of tip Mach number and divergence on blade twist.

Twist at Low Tip Mach Numbers

Some causes of blade twist.- The data points presented in figure 17 were obtained by varying the density at constant rotor speed to eliminate the effect of Mach number on twist. In addition to the aerodynamic forces and moments which produce twist, there are also body forces and moments due to the spanwise and chordwise components of the centrifugal acceleration of the blade mass particles, references 10 and 11. The spanwise components result in so-called "ribbon forces" which tend to minimize blade twist in either positive or negative directions. The resulting moments are directly proportional to the blade twist and are, therefore, negligible if the twist is negligible. The chordwise components produce moments which are proportional to the sine of twice the pitch angle, the direction of which is such as to restore the pitch angle to zero. If these moments are significant for the blade in question, they should show up at the high pitch angles and would result in negative blade twist at zero density. The data presented in figure 17 for pitch angle settings of 15°, 17.5°, and 20° indicate that the twist at zero density is nearly zero (as shown by the dashed lines). Since this appears to be true for high pitch angles, it seems reasonable that the curves for low pitch angles would follow the trend indicated by the

dashed lines in showing zero twist at zero density. Thus, it is concluded for these blades that the effects of centrifugal forces on blade twist are small compared to the aerodynamic forces.

Effect of blade pitch angle.- The data also show that as the pitch angle is increased from zero, the angle of twist, at a given value of dynamic pressure, also increases. This trend continues, as shown by the cross-plotted data of figure 18 until the pitch angle approaches approximately 15°, whereupon further increases in the pitch angle result in a reduction in twist. As the pitch angle approaches an angle of 25°, the blade twist is zero, indicating that the center of pressure has moved rearward and has become coincident with the center of gravity. As the pitch angle is further increased, the center of pressure apparently moves rearward of the center of gravity and the twist becomes negative.

With the exception of the blade-pitch-angle setting of 5°, the maximum value of the dynamic pressure for each blade-pitch-angle setting of the curves in figure 17 is slightly less than the dynamic pressure at which flutter occurred. No flutter was obtained at the blade-pitch-angle setting of 5°; however, the curve does show a tendency toward divergence. The limiting value of the dynamic pressure was due to the limit on the rotor speed imposed by centrifugal stresses. If flutter had occurred, it is likely that, at this relatively low pitch angle, it would have been of the classical bending-torsion type.

Theoretical prediction of twist and divergence.- An attempt is made in the following paragraphs to show how the theory of references 7 and 9 may be applied to predict the divergence tendency exhibited by the blade in figure 17 at the 5° pitch-angle setting. The theory is advanced in reference 7 that the dynamic-stiffness axis may be taken as the center of gravity of the section and the divergence speed will be approximately equal to the classical flutter speed. The approximate classical flutter speed coefficient for a heavy wing with a low bending-to-torsion frequency ratio (a condition which is met by the rotor blade under consideration) was derived in reference 9 and repeated in a more convenient form in reference 7. Assuming that the effective velocity is the velocity at 0.8R, the flutter speed coefficient may be written in the modified form as follows:

$$\frac{V_{0.8R}}{b\omega_\alpha}\sqrt{\frac{\rho}{\rho_o}} = \sqrt{\frac{r_\alpha^2}{\kappa_o}\,\frac{1/4}{x_{cg} - 1/4}} \tag{1}$$

where the subscript o is used to designate standard atmospheric conditions.

By substituting the appropriate values from table I for blade 3(r) into equation (1), the critical value of $(V_{0.8R}/b\omega_\alpha)\sqrt{\rho/\rho_o}$ was determined to be 6.1 which indicates that the classical flutter or divergence speed coefficient of the blade was just slightly greater than the maximum value shown in figure 17.

According to reference 7, for small pitch angles the ratio of blade twist at successive dynamic pressures (designated by subscripts 1 and 2) may be expressed as

$$\frac{\Delta\theta_1}{\Delta\theta_2} = \frac{\dfrac{q_1/q_{cr}}{1 - \dfrac{q_1}{q_{cr}}}}{\dfrac{q_2/q_{cr}}{1 - \dfrac{q_2}{q_{cr}}}} \tag{2}$$

where q_{cr} is the dynamic pressure at flutter or divergence. Inasmuch as $\left(\frac{V_{0.8R}}{b\omega_\alpha}\right)^2 \frac{\rho}{\rho_o} \Bigg/ \left[\left(\frac{V_{0.8R}}{b\omega_\alpha}\right)^2 \frac{\rho}{\rho_o}\right]_{cr} = q/q_{cr}$, the ratio of successive values of blade twist for corresponding values of the flutter speed coefficient becomes, after substitution of the critical values of $(V_{0.8R}/b\omega_\alpha)^2(\rho/\rho_o)$,

$$\left(\Delta\theta_t\right)_2 = \left(\Delta\theta_t\right)_1 \frac{\left[\left(\frac{V_{0.8R}}{b\omega_\alpha}\right)^2 \frac{\rho}{\rho_o}\right]_2 \left\{37.2 - \left[\left(\frac{V_{0.8R}}{b\omega_\alpha}\right)^2 \frac{\rho}{\rho_o}\right]_1\right\}}{\left[\left(\frac{V_{0.8R}}{b\omega_\alpha}\right)^2 \frac{\rho}{\rho_o}\right]_1 \left\{37.2 - \left[\left(\frac{V_{0.8R}}{b\omega_\alpha}\right)^2 \frac{\rho}{\rho_o}\right]_2\right\}} \tag{3}$$

where the constant 37.2 is the square of the critical value of the flutter speed coefficient as previously determined from equation (1) for the particular blade under consideration.

Comparison of theory and experiment.- Figure 19 presents a comparison of some theoretical and experimental values of blade twist as a function of flutter speed coefficient as the calculated divergence speed is approached. The curve of measured twist against flutter speed coefficient shown in figure 17 for a blade-pitch-angle setting of 5° is repeated along with two calculated curves, one of which is obtained from equation (3) and the other based on the assumption that the twist is directly proportional to the dynamic pressure, that is,

$$(\Delta\theta_t)_2 = (\Delta\theta_t)_1 \frac{\left[\left(\frac{V_{0.8R}}{b\omega_\alpha}\right)^2 \frac{\rho}{\rho_o}\right]_2}{\left[\left(\frac{V_{0.8R}}{b\omega_\alpha}\right)^2 \frac{\rho}{\rho_o}\right]_1} \tag{4}$$

In both instances, the initial values of blade twist and flutter speed coefficient for the calculated curves are assumed to be equal to the experimental values of $\Delta\theta_t = 0.61$ and $\left(V_{0.8R}/b\omega_\alpha\right)\sqrt{\rho/\rho_o} = 3$. If no experimental value of twist is available, the twist may be determined from equation (3) of reference 7.

A comparison of the three curves of figure 19 shows a definite tendency of the blade toward divergence; however, the twist is not quite as great as the theory predicts, the theory being, in this case, somewhat conservative. This may be attributed partly to the increase in blade stiffness arising from centrifugal forces and, perhaps, partly to violation of the small-angle limitation of the theory.

Effect of Tip Mach Number on Blade Twist

Figures 20 and 21 show the effect of the flutter speed coefficient and blade tip Mach number on the twist of a 12-percent-thick blade operating in mediums having different speeds of sound. The chordwise center of gravity was located at 37.3 percent chord and the blade pitch angle was set at 5°. The data are presented in tabular form in table III.

Figure 20 shows the blade twist as a function of the flutter speed coefficient. The curves for the test mediums having the higher sound speeds show a tendency toward divergence at a value of $\left(V_{0.8R}/b\omega_\alpha\right)\sqrt{\rho/\rho_o}$ from 3.5 to 4 whereas the curves at low sound speeds show a turnback

or reduction in twist, probably due to the effect of a rearward movement of the center of pressure as a result of the increase in Mach number. The effect of Mach number is more conveniently shown in figure 21 where the blade twist, divided by the value of the flutter speed coefficient at which it was obtained, is plotted as a function of the tip Mach number.

The curves representing data at the higher sound speeds again show a tendency toward divergence as discussed in the previous paragraph. Since this divergent tendency, as shown in figure 20, occurred at essentially constant dynamic pressure in mediums having different sound speeds, it occurs at different tip Mach numbers. As the sound speed is progressively lowered, the divergence tendency disappears and a Mach number effect becomes evident. As the Mach number approaches 0.73, a turnback in the twist curves is shown and indicates a reduction in twist with further increases in tip Mach number. The Mach number at which the turnback occurs is in agreement with the limiting Mach number of the envelope flutter boundary of figure 11(a), a fact which may indicate that the rise in the value of the flutter speed coefficient at high Mach numbers is partially due to a rearward shift of the center of pressure as evidenced by a reduction in blade pitch angle.

REFERENCES

1. Brooks, George W., and Sylvester, Maurice A.: Description and Investigation of a Dynamic Model of the XH-17 Two-Blade Jet-Driven Helicopter. NACA RM L50I21, 1951.

2. Baker, John E.: The Effects of Various Parameters, Including Mach Number, on Propeller-Blade Flutter With Emphasis on Stall Flutter. NACA TN 3357, 1955. (Supersedes NACA RM L50L12b.)

3. Rainey, A. Gerald: Preliminary Study of Some Factors Which Affect the Stall-Flutter Characteristics of Thin Wings. NACA TN 3622, 1956. (Supersedes NACA RM L52D08.)

4. Turner, M. J., and Duke, James B.: Propeller Flutter. Jour. Aero. Sci., vol. 16, no. 6, June 1949, pp. 323-336.

5. Rosenberg, Reinhardt: Aero-Elastic Instability in Unbalanced Lifting Rotor Blades. Jour. Aero. Sci., vol. 11, no. 4, Oct. 1944, pp. 361-368.

6. Glauert, H.: The Elements of Aerofoil and Airscrew Theory. Second ed., Cambridge Univ. Press, reprint of 1947, p. 215.

7. Theodorsen, Theodore, and Regier, Arthur A.: Effect of the Lift Coefficient on Propeller Flutter. NACA WR L-161, 1945. (Formerly NACA ACR L5F30.)

8. Allis, Arthur E., and Swihart, John M.: The Effect of Blade-Section Camber on the Stall-Flutter Characteristics of Three NACA Propellers at Zero Advance. NACA RM I53B17, 1953.

9. Theodorsen, Theodore, and Garrick, I. E.: Mechanism of Flutter - A Theoretical and Experimental Investigation of the Flutter Problem. NACA Rep. 685, 1940.

10. Sterne, L. H. G.: The Structural Aspects of Propeller Design. Rep. No. Structures 5, British R.A.E., July 1947.

11. Biot, M. A.: Increase of Torsional Stiffness of a Prismatical Bar Due to Axial Tension. Jour. Appl. Phys., vol. 10, no. 12, Dec. 1939, pp. 860-864.

TABLE I.- CHARACTERISTIC BLADE PARAMETERS

[Hub radius, 8 inches; rotor radius, 46 inches; flapping hinge radius, 2.5 inches]

(a) NACA 23012 airfoil section

Blade number	1(r)	2(f)	2(r)	3(f)	3(r)	4(r)	5(r)
Length, in.	38	38	38	38	38	38	38
Chord, in.	4	4	4	4	4	4	4
x_{cg}, percent chord	37.3	27.5	37.3	27.5	37.3	37.3	37.3
x_{EA}, percent chord	26.5	25.0	26.5	25.0	26.5	26.5	26.5
GJ, lb-in.^{2}	9,980	8,260	9,210	7,800	7,900	8,210	9,980
EI, lb-in.^{2}	25,500	25,500	25,500	24,300	24,300	24,300	24,300
ω_{h_1}, radians/sec	126	113	119	129	116	126	126
ω_{h_2}, radians/sec	327	319	331	364	327	327	327
ω_α, radians/sec	464	439	446	426	414	421	464
r_α^2	0.235	0.165	0.235	0.165	0.235	0.235	0.235
$(1/\kappa)_o$	78.0	78.0	78.0	78.0	78.0	78.0	78.0
g_{h_1}	0.126	0.105	0.110	0.134	0.093	0.170	0.135
g_{h_2}	0.049	0.036	0.040	------	0.035	0.056	0.067
g_α	0.048	0.093	0.075	0.027	0.034	0.049	0.067
m_r, slugs	0.181	0.181	0.181	0.181	0.181	0.181	0.181
I_r, slug-ft^2	0.0055	0.0055	0.0055	0.0055	0.0055	0.0055	0.0055
σ	0.028	0.028	0.028	0.028	0.028	0.028	0.028
γ_o	3.695	3.695	3.695	3.695	3.695	3.695	3.695

(b) NACA 23018 airfoil section

Blade number	6(f)	6(r)	7(r)	8(r)	9(r)
Length, in.	38	38	38	38	38
Chord, in.	4	4	4	4	4
x_{cg}, percent chord	28.0	36.5	36.5	36.5	36.5
x_{EA}, percent chord	25.0	27.0	27.0	27.0	27.0
GJ, lb-in.^{2}	18,650	20,400	14,150	16,950	16,950
EI, lb-in.^{2}	59,100	59,100	57,800	67,900	67,900
ω_{h_1}, radians/sec	173	168	151.0	180	180
ω_{h_2}, radians/sec	477	458	454	488	488
ω_α, radians/sec	611	616	513	576	562
r_α^2	0.168	0.216	0.216	0.216	0.216
$(1/\kappa)_o$	88.1	88.1	88.1	88.1	88.1
g_{h_1}	0.045	0.076	0.054	0.051	0.051
g_{h_2}	0.015	0.044	0.042	0.059	0.059
g_α	0.064	0.069	0.062	0.054	0.224
m_r, slugs	0.181	0.181	0.181	0.181	0.181
I_r, slug-ft^2	0.0055	0.0055	0.0055	0.0055	0.0055
σ	0.028	0.028	0.028	0.028	0.028
γ_o	3.275	3.275	3.275	3.275	3.275

TABLE II.- TABULATION OF FLUTTER DATA

$(\theta_{0.8R})_s$, deg	V_t, ft/sec	c, ft/sec	M_t	$\sqrt{\frac{\rho}{\rho_o}}$	$\frac{V_{0.8R}}{b\omega_T}$	$\frac{V_{0.8R}}{b\omega_T}\sqrt{\frac{\rho}{\rho_o}}$	ω_T, radians/sec	Mean $\Delta\theta_t$, deg	Characteristics of flutter
NACA 23012, blade 1(r)									
2.0	574	1143	0.502	0.984	5.94	5.84	320	0.5	Sustained
3.4	553	1157	.478	.972	5.72	5.56	331	---	Fluttered - to destruction
4.0	548	1150	.476	.980	5.67	5.56	337	4.5	Sustained
4.0	536	1150	.466	.980	5.54	5.43	335	4.5	Sustained
5.8	535	1148	.466	.980	5.53	5.42	336	7.8	Sustained
8.7	417	1152	.362	.977	4.31	4.21	397	5.1	Sustained
12.8	305	1152	.265	.977	3.15	3.08	407	2.2	Sustained
17.2	210	1151	.182	.977	2.17	2.12	433	.8	Sustained
22.3	191	1152	.166	.977	1.98	1.93	444	-1.8	Intermittent
26.8	186	1154	.161	.975	1.92	1.87	455	-2.8	Sustained
32.6	380	1159	.328	.971	3.93	3.81	---	-3.1	No flutter to V_t
NACA 23012, blade 2(f)									
9.1	500	1131	0.442	0.995	5.45	5.43	---	2.0	No flutter to V_t
11.1	477	1131	.422	.995	5.22	5.20	525	1.3	Sustained
	482	1130	.427	.996	5.29	5.00	519		Sustained
	516	1130	.457	.902	5.65	5.09	521		Sustained
	500	510	.980	1.035	5.47	5.67	---		No flutter to V_t
	500	523	.956	1.054	5.47	5.76	---		No flutter to V_t
	500	547	.914	1.068	5.47	5.84	---		No flutter to V_t
	407	567	.718	1.078	4.47	4.81	546		Intermittent
	407	585	.696	1.092	4.45	4.86	540		Intermittent
	413	600	.688	1.115	4.53	5.05	565		Intermittent
	386	600	.643	1.115	4.21	4.70	519		Intermittent
	402	600	.670	1.115	4.41	4.91	528		Sustained
	500	620	.807	1.020	5.49	5.60	---		No flutter to V_t
	444	640	.694	1.025	4.89	5.01	565		*Sustained

*Top of flutter region.

TABLE II.- TABULATION OF FLUTTER DATA - Continued

$(\theta_{0.8R})_s$, deg	V_t, ft/sec	c, ft/sec	M_t	$\sqrt{\frac{\rho}{\rho_o}}$	$\frac{V_{0.8R}}{b\omega_\alpha}$	$\frac{V_{0.8R}}{b\omega_\alpha}\sqrt{\frac{\rho}{\rho_o}}$	ω_f, radians/sec	Mean $\Delta\theta_t$, deg	Characteristics of flutter
NACA 23012, blade 2(f) - continued									
11.1	402	640	0.628	1.025	4.41	4.52	503	1.3	Sustained
	436	640	.681	.950	4.75	4.52	546		Intermittent
	391	665	.588	1.055	4.30	4.53	509		Sustained
	412	665	.620	1.055	4.52	4.77	528		Sustained
	465	665	.699	1.055	5.09	5.37	578		*Intermittent
	417	665	.627	1.006	4.58	4.60	522		Sustained
	446	665	.671	1.006	4.89	4.91	565		*Sustained
	407	668	.704	.940	5.14	4.83	606		Intermittent
	405	705	.575	1.080	4.42	4.78	512		Sustained
	453	705	.643	1.080	4.94	5.34	571		*Sustained
	422	710	.594	.977	4.60	4.49	516		Intermittent
	413	750	.551	1.016	4.66	4.74	490		Sustained
	420	750	.560	.977	4.59	4.48	509		Sustained
	482	750	.643	.908	5.43	4.93	555		Intermittent
14.8	338	1142	.296	.990	3.69	3.65	477	.3	Sustained
	352	1141	.307	.919	3.82	3.53	489		Sustained
	371	1140	.325	.832	4.05	3.37	496		Sustained
	451	1137	.396	.760	4.94	3.75	521		Sustained
	495	1139	.435	.696	5.45	3.77	515		Sustained
	328	494	.664	1.036	3.61	3.74	515		Sustained
	362	494	.733	1.036	3.99	4.14	565		*Intermittent
	301	495	.608	.978	3.29	3.22	508		Sustained
	352	495	.711	.978	3.84	3.76	558		*Intermittent
	338	497	.680	.892	3.70	3.30	527		Sustained
	362	497	.728	.892	3.97	3.54	565		*Intermittent
	314	497	.632	.805	3.43	2.76	502		Sustained
	328	497	.660	.805	3.59	2.89	521		*Sustained
	289	537	.538	1.025	3.16	3.24	490		Sustained

*Top of flutter region.

TABLE II.- TABULATION OF FLUTTER DATA - Continued

$(\theta_{0.8R})_s$, deg	V_t, ft/sec	c, ft/sec	M_t	$\sqrt{\frac{\rho}{\rho_o}}$	$\frac{V_{0.8R}}{b\omega_\alpha}$	$\frac{V_{0.8R}}{b\omega_\alpha}\sqrt{\frac{\rho}{\rho_o}}$	ω_T, radians/sec	Mean $\Delta\theta_t$, deg	Characteristics of flutter
NACA 23012, blade 2(f) - concluded									
14.8	372	537	0.693	1.025	4.07	4.17	558	0.3	*Sustained
	323	537	.601	.931	3.53	3.29	502		Sustained
	381	537	.709	.931	4.17	3.88	558		*Sustained
	338	537	.629	.860	3.70	3.18	512		Sustained
	362	537	.674	.860	3.95	3.40	527		*Sustained
	338	537	.629	.786	3.70	2.91	502		Sustained
	352	537	.656	.786	3.86	3.03	515		*Sustained
	309	595	.515	1.000	3.38	3.38	489		Sustained
	388	595	.652	1.000	4.25	4.25	571		*Sustained
	328	595	.551	.944	3.58	3.38	502		Sustained
	388	595	.652	.944	4.23	3.99	---		*Sustained
	336	595	.565	.865	3.67	3.17	---		Sustained
	352	595	.592	.785	3.85	3.02	---		Sustained
	372	595	.625	.785	4.07	3.19	---		*Sustained
	304	660	.461	1.040	3.33	3.47	---		Sustained
	280	660	.424	1.040	3.06	3.18	---		Sustained
	320	660	.485	0.956	3.50	3.35	---		Sustained
	345	660	.527	.880	3.77	3.32	502		Sustained
	386	663	.582	.786	3.74	3.31	515		Sustained
19.1	239	1129	.212	1.000	2.62	2.62	465	-.6	Sustained
	251	1129	.222	.938	2.74	2.57	458		Sustained
	263	1129	.233	.875	2.88	2.52	458		Sustained
	313	1126	.278	.795	3.43	2.72	470		Sustained
	345	1128	.306	.717	3.78	2.71	470		Sustained
24.6	263	1139	.231	.990	2.88	2.85	465	-3.1	Sustained
	301	1142	.264	.919	3.29	3.02	470		Intermittent

*Top of flutter region.

TABLE II.- TABULATION OF FLUTTER DATA - Continued

$(\theta_{0.8R})_B$, deg	V_t, ft/sec	c, ft/sec	M_t	$\sqrt{\rho/\rho_0}$	$\frac{V_{0.8R}}{b\omega_\alpha}$	$\frac{V_{0.8R}}{b\omega_\alpha}\sqrt{\rho/\rho_0}$	ω_β, radians/sec	Mean $\Delta\theta_t$, deg	Characteristics of flutter
NACA 23012, blade 2(r)									
7.2	491	1135	0.433	0.985	5.28	5.20	396	4.1	Sustained
	500	1133	.441	.895	5.37	4.82	---		No flutter to V_t
	495	1134	.437	.923	5.32	4.91	400		Sustained
	500	498	1.004	.995	5.37	5.35	---		No flutter to V_t
	500	528	.947	1.005	5.37	5.40	---		No flutter to V_t
	500	542	.923	1.030	5.37	5.50	---		No flutter to V_t
	390	569	.685	1.040	4.19	4.36	411		Sustained
	376	569	.661	1.040	4.04	4.20	386		Intermittent
	368	571	.644	1.110	3.95	4.38	---		Sustained
	381	580	.657	1.028	4.09	4.21	387		Sustained
	402	580	.693	1.028	4.32	4.45	409		*Sustained
	500	585	.855	.929	5.37	5.00	---		No flutter to V_t
	430	645	.667	.966	4.62	4.46	---		Sustained
	500	648	.772	.894	5.37	4.80	---		No flutter to V_t
	468	1125	.416	1.000	5.04	5.04	383		Sustained
	498	1125	.443	.948	5.35	5.07	386		Sustained
11.2	362	1145	.316	.979	3.89	3.81	415	1.7	Sustained
	414	1145	.362	.894	4.45	3.98	428		Sustained
	458	1145	.400	.802	4.92	3.95	440		Sustained
	492	1147	.429	.753	5.29	3.98	446		Sustained
	318	527	.603	.971	3.42	3.32	411		Sustained
	322	533	.604	1.010	3.46	3.49	411		Sustained
	351	539	.651	.903	3.77	3.40	433		Sustained
	371	542	.684	.783	3.99	3.12	452		Sustained
	328	604	.543	1.000	3.52	3.52	415		Sustained
	353	607	.582	.930	3.79	3.52	427		Sustained
	373	608	.613	.871	4.01	3.49	440		Sustained
	390	608	.641	.783	4.19	3.28	452		Sustained

*Top of flutter region.

TABLE II.- TABULATION OF FLUTTER DATA - Continued

$(\theta_{0.8R})_s$, deg	V_t, ft/sec	c, ft/sec	M_t	$\sqrt{\rho/\rho_0}$	$\frac{V_{0.8R}}{b\omega_\alpha}$	$\frac{V_{0.8R}}{b\omega_\alpha}\sqrt{\rho/\rho_0}$	ω_r, radians/sec	Mean $\Delta\beta_t$, deg	Characteristics of flutter
NACA 23012, blade 2(r) - continued									
11.2	404	608	0.664	0.745	4.34	3.23	472	1.7	Sustained
	347	699	.496	.991	3.73	3.70	427		Sustained
	403	709	.568	.903	4.33	3.91	440		Sustained
	403	709	.568	.840	4.33	3.64	440		Sustained
	408	709	.575	.792	4.38	3.47	446		Sustained
	425	712	.597	.728	4.57	3.33	449		Sustained
	446	716	.623	.659	4.79	3.16	462		Sustained
	385	1135	.339	.984	4.14	4.07	434		Sustained
	420	1134	.370	.885	4.51	3.99	440		Sustained
	468	1133	.413	.800	5.03	4.02	446		Sustained
	500	1133	.441	.690	5.37	3.71	---		No flutter to V_t
	500	1133	.441	.719	5.37	3.86	---		No flutter to V_t
	499	1134	.440	.743	5.36	3.98	459		Sustained
16.2	240	1154	.208	.972	2.58	2.51	409	0.3	Sustained
	266	1148	.231	.848	2.86	2.43	413		Sustained
	330	1150	.287	.693	3.55	2.46	423		Sustained
	271	532	.510	.952	2.92	2.78	418		Sustained
	261	545	.478	.826	2.81	2.32	414		Sustained
	315	556	.566	.665	3.38	2.25	418		Sustained
	346	565	.613	.605	3.72	2.25	437		Sustained
	500	566	.883	.558	5.39	3.01	---		No flutter to V_t
	250	594	.421	.990	2.70	2.67	404		Sustained
	226	595	.380	.990	2.43	2.41	400		Sustained
	265	601	.441	.839	2.86	2.40	418		Sustained
	313	604	.518	.693	3.36	2.33	433		Sustained
	224	679	.330	.990	2.41	2.39	396		Sustained
	258	674	.380	.852	2.78	2.37	409		Sustained
	320	685	.467	.672	3.45	2.32	423		Sustained

TABLE II.- TABULATION OF FLUTTER DATA - Continued

$(\theta_{0.8R})_s$, deg	V_t, ft/sec	a, ft/sec	M_t	$\sqrt{\frac{\rho}{\rho_o}}$	$\frac{V_{0.8R}}{b\omega_\alpha}$	$\frac{V_{0.8R}}{b\omega_\alpha}\sqrt{\frac{\rho}{\rho_o}}$	ω_f, radians/sec	Mean $\Delta\theta_t$, deg	Characteristics of flutter
NACA 23012, blade 2(r) - concluded									
21.7	268	1145	0.234	0.975	2.89	2.82	428	-1.6	Sustained
	231	1150	.201	.975	2.53	2.47	423		Sustained
	255	1150	.222	.975	2.75	2.67	423		Sustained
	361	1150	.314	.808	3.88	3.14	453		Sustained
	466	1152	.405	.713	5.02	3.58	470		Sustained
	289	527	.548	.961	3.11	2.99	423		Sustained
	482	531	.908	.858	5.19	4.45	---		No flutter to V_t
	285	535	.533	.899	3.06	2.75	428		Sustained
	292	539	.542	.871	3.14	2.74	437		Sustained
	257	630	.408	.994	2.77	2.75	419		Sustained
	286	630	.454	.885	3.08	2.73	428		Sustained
	482	610	.791	.750	5.18	3.89	---		No flutter to V_t
	482	619	.780	.808	5.18	4.19	---		No flutter to V_t
	298	622	.479	.864	3.21	2.77	438		Sustained
	263	719	.366	.994	2.82	2.80	427		Sustained
	292	721	.405	.820	3.14	2.58	428		Sustained
	290	705	.412	.895	3.14	2.81	428		Sustained
NACA 23012, blade 3(f)									
14.3	486	520	0.935	0.930	5.47	5.09	---	1.2	No flutter to V_t
	492	590	.834	.974	5.54	5.40	---		No flutter to V_t
	361	650	.556	1.024	4.06	4.16	489		Sustained
	433	650	.666	1.024	4.88	5.00	533		*Sustained
	394	630	.625	.976	4.44	4.33	502		*Sustained
	394	630	.625	.976	4.44	4.33	502		Sustained
	364	740	.492	.986	4.10	4.04	483		Sustained
	361	810	.446	.990	4.07	4.03	477		Sustained
	377	1154	.327	.970	4.25	4.12	483		Sustained

*Top of flutter region.

TABLE II.- TABULATION OF FLUTTER DATA - Continued

$(\theta_{0.8R})_g$, deg	V_t, ft/sec	c, ft/sec	M_t	$\sqrt{\frac{\rho}{\rho_0}}$	$\frac{V_{0.8R}}{b\omega_\alpha}$	$\frac{V_{0.8R}}{b\omega_\alpha}\sqrt{\frac{\rho}{\rho_0}}$	ω_r, radians/sec	Mean $\Delta\theta_t$, deg	Characteristics of flutter
NACA 23012, blade 3(f) - concluded									
17.4	203	510	0.398	0.980	2.29	2.24	452	0.5	Sustained
	220	515	.427	.901	2.48	2.23	464		Sustained
	208	515	.404	.901	2.34	2.11	458		Sustained
	229	515	.445	.826	2.58	2.13	464		Sustained
	250	520	.481	.726	2.82	2.05	464		Sustained
	390	525	.743	.646	4.39	2.84	---		No flutter to V_t
	309	525	.589	.688	3.48	2.39	489		Sustained
	321	525	.612	.688	3.62	2.49	496		*Sustained
	228	1133	.201	.988	2.57	2.54	464		Sustained
19.2	187	1135	.165	.987	2.11	2.08	439	0.1	Sustained
20.0	168	1135	.148	.987	1.89	1.87	439	0	Sustained
20.2	148	1135	.130	.987	1.67	1.65	433	0	Sustained
21.5	143	1135	.126	.987	1.61	1.59	446	-.2	Sustained
	202	530	.381	.566	2.27	1.28	452		Sustained
	330	530	.623	.566	3.72	2.11	502		*Sustained
	222	535	.415	.536	2.50	1.34	470		Sustained
	162	980	.165	.717	1.82	1.31	451		Sustained
	315	535	.589	.536	3.55	1.90	489		*Sustained
	198	660	.300	.616	2.23	1.37	464		Sustained
	179	750	.239	.674	2.02	1.36	458		Sustained
25.8	156	1135	.137	.987	1.76	1.74	452	-1.2	Sustained
NACA 23012, blade 3(r)									
5.0	481	1135	0.424	1.000	5.58	5.58	---	5.0	No flutter to V_t
10.2	349	1156	.302	.969	4.05	3.92	402	4.5	Sustained
	481	560	.859	.781	5.58	4.36	---		No flutter to V_t
	481	605	.795	.818	5.58	4.57	---		No flutter to V_t
	392	630	.622	.842	4.54	3.82	427		Sustained

*Top of flutter region.

TABLE II.- TABULATION OF FLUTTER DATA - Continued

$(\theta_{0.8R})_s$, deg	V_t, ft/sec	c, ft/sec	M_t	$\sqrt{\frac{\rho}{\rho_o}}$	$\frac{V_{0.8R}}{b\omega_\alpha}$	$\frac{V_{0.8R}}{b\omega_\alpha}\sqrt{\frac{\rho}{\rho_o}}$	ω_r, radians/sec	Mean $\Delta\theta_t$, deg	Characteristics of flutter
NACA 23012, blade 3(r) - concluded									
10.2	447	630	0.708	0.842	5.18	4.36	458	4.5	*Sustained
↓	380	670	.567	.853	4.41	3.77	427	↓	Sustained
	337	760	.444	.968	3.91	3.79	402		Sustained
	334	835	.400	.985	3.87	3.81	396		Sustained
15.2	201	1130	.178	.992	2.33	2.31	389	2.0	Sustained
↓	211	510	.413	.798	2.45	1.96	408	↓	Sustained
	221	515	.428	.712	2.56	1.82	405		Sustained
	233	515	.452	.674	2.70	1.82	408		Sustained
	254	520	.488	.628	2.94	1.85	411		Sustained
	349	520	.671	.628	4.05	2.54	---		*Sustained
	441	530	.832	.522	5.11	2.67	---		No flutter to V_t
	441	530	.832	.566	5.11	2.89	---		No flutter to V_t
	257	525	.490	.598	2.98	1.78	---		Sustained
	289	525	.550	.598	3.35	2.00	---		*Sustained
	237	710	.334	.736	2.75	2.02	---		Sustained
↓	213	830	.257	.857	2.56	2.19	---	↓	Sustained
17.5	156	1135	.138	1.000	1.81	1.81	---	1.4	Sustained
20.0	141	1135	.124	1.000	1.63	1.63	---	.5	Sustained
24.0	120	1128	.107	.996	1.39	1.38	---	.3	Sustained
↓	129	505	.256	.950	1.50	1.42	---	↓	Sustained
	147	510	.288	.646	1.70	1.10	---		Sustained
28.0	129	1135	.114	1.000	1.50	1.50	---	.0	Sustained
32.0	201	1135	.177	1.000	2.33	2.33	---	-.9	No flutter to V_t

*Top of flutter region.

TABLE II.- TABULATION OF FLUTTER DATA - Continued

$(\theta_{0.8R})_s$, deg	V_t, ft/sec	c, ft/sec	M_t	$\sqrt{\frac{\rho}{\rho_o}}$	$\frac{V_{0.8R}}{b\omega_\alpha}$	$\frac{V_{0.8R}}{b\omega_\alpha}\sqrt{\frac{\rho}{\rho_o}}$	ω_f, radians/sec	Mean $\Delta\theta_t$, deg	Characteristics of flutter
NACA 23012, blade 4(r)									
8.1	436	1149	0.293	0.975	4.97	4.84	386	6.9	Sustained
10.6	359	1152	.336	.973	4.09	3.98	393	4.9	Sustained
13.7	280	1150	.187	.975	3.19	3.11	396	3.2	Sustained
16.0	215	1152	.141	.973	2.45	2.39	393	2.1	Sustained
18.7	167	1151	.111	.974	1.90	1.85	389	1.0	Sustained
18.7	169	1151	.112	.974	1.93	1.88	396	1.0	Sustained
21.7	152	1151	.101	.974	1.73	1.68	402	0	Sustained
21.7	160	1151	.106	.974	1.82	1.77	396	0	Sustained
24.7	165	1151	.109	.974	1.88	1.83	393	-.7	Sustained
NACA 23012, blade 5(r)									
8.1	460	1148	0.401	0.976	4.76	4.65	408	6.5	Sustained
10.6	384	1139	.338	.983	3.97	3.90	423	5.8	Intermittent
15.0	277	1141	.243	.982	2.87	2.82	423	3.1	Intermittent
15.0	278	1141	.244	.982	2.88	2.83	417	3.1	Sustained
18.2	241	1147	.210	.977	2.50	2.44	414	1.3	Sustained
20.0	235	1142	.206	.980	2.43	2.38	420	.6	Sustained
20.0	233	1142	.204	.980	2.41	2.36	465	.6	Intermittent
22.5	242	1145	.212	.978	2.50	2.45	414	0	Sustained
25.0	321	1143	.281	.979	3.32	3.25	---	0	No flutter to V_t

TABLE II.- TABULATION OF FLUTTER DATA - Continued

$(\theta_{0.8R})_s$, deg	V_t, ft/sec	c, ft/sec	M_t	$\sqrt{\frac{\rho}{\rho_o}}$	$\frac{V_{0.8R}}{b\omega_\alpha}$	$\frac{V_{0.8R}}{b\omega_\alpha}\sqrt{\frac{\rho}{\rho_o}}$	ω_f, radians/sec	Mean $\Delta\theta_t$, deg	Characteristics of flutter
NACA 23018, blade 6(f)									
16	567	1111	0.510	1.007	4.45	4.49	690	1.4	Intermittent
	383	555	.690	.919	3.01	2.77	655		*Intermittent
	359	555	.647	.919	2.82	2.59	652		Intermittent
	343	544	.631	1.003	2.69	2.70	625		Intermittent
	368	544	.676	1.003	2.89	2.90	654		*Intermittent
	429	606	.708	1.046	3.37	3.53	677		*Intermittent
	362	606	.597	1.046	2.84	2.98	616		Intermittent
	387	660	.586	1.099	3.04	3.34	616		Intermittent
	453	660	.686	1.099	3.56	3.91	704		*Intermittent
	413	734	.563	1.183	3.24	3.84	647		Intermittent
	440	734	.599	1.183	3.46	4.09	672		Sustained
	422	734	.575	.983	3.31	3.26	628		Sustained
	402	734	.548	.858	3.16	2.71	608		Sustained
	446	830	.537	.979	3.50	3.43	622		Intermittent
	468	860	.544	1.034	3.68	3.80	613		Intermittent
18	418	1101	.379	1.019	3.28	3.35	650	1.0	Sustained
	513	1101	.466	.836	4.03	3.37	664		Sustained
	516	1101	.468	.836	4.05	3.39	672		Sustained
	413	548	.754	1.071	3.24	3.48	734		*Intermittent
	381	548	.695	1.071	2.99	3.21	685		Intermittent
	340	574	.592	1.091	2.67	2.92	660		*Intermittent
	335	574	.584	1.091	2.63	2.87	679		Intermittent
	373	574	.650	1.091	2.93	3.20	628		*Intermittent
	348	625	.557	1.134	2.73	3.10	628		Sustained
	389	625	.622	1.134	3.06	3.47	686		*Sustained
	422	625	.675	.981	3.32	3.25	657		*Intermittent
	349	625	.558	.981	2.74	2.69	628		Intermittent
	452	720	.628	1.062	3.55	3.77	702		*Sustained
	388	720	.539	1.062	3.05	3.24	647		Sustained

* Top of flutter region.

TABLE II.- TABULATION OF FLUTTER DATA - Continued

$(\theta_{0.8R})_s$, deg	V_t, ft/sec	c, ft/sec	M_t	$\sqrt{\frac{\rho}{\rho_o}}$	$\frac{V_{0.8R}}{b\omega_\alpha}$	$\frac{V_{0.8R}}{b\omega_\alpha}\sqrt{\frac{\rho}{\rho_o}}$	ω_f, radians/sec	Mean $\Delta\theta_t$, deg	Characteristics of flutter
NACA 23018, blade 6(f) - continued									
18	362	780	0.464	1.145	2.84	3.26	628	1.0	Sustained
	407	780	.522	.988	3.20	3.16	655		Intermittent
	424	780	.544	.988	3.33	3.29	660		*Sustained
	545	490	1.111	1.056	4.28	4.53	---		No flutter to V_t
	395	840	.470	1.072	3.10	3.33	663		Intermittent
	403	840	.480	1.072	3.17	3.40	628		Sustained
	410	840	.488	1.001	3.22	3.23	637		Sustained
	495	840	.589	1.001	3.89	3.90	680		*Intermittent
	471	840	.561	1.001	3.70	3.71	684		*Sustained
20	336	1120	.300	1.003	2.64	2.65	612	0.4	Sustained
	425	1120	.379	.751	3.34	2.51	660		Intermittent
	520	1120	.464	.751	4.08	3.07	672		Intermittent
	304	1120	.450	.751	3.96	2.97	652		Sustained
	282	560	.504	1.075	2.22	2.38	605		Sustained
	275	560	.491	1.075	2.16	2.32	602		*Sustained
	418	1120	.373	.751	3.28	2.46	654		Sustained
	286	560	.511	1.075	2.25	2.42	602		*Sustained
	296	664	.446	1.158	2.33	2.69	595		Sustained
	322	664	.485	.994	2.53	2.52	622		Intermittent
	306	664	.461	.994	2.40	2.39	597		Sustained
	310	664	.467	.994	2.44	2.42	612		Intermittent
	301	664	.453	.994	2.36	2.35	612		Intermittent
	306	735	.416	1.085	2.40	2.61	597		Sustained
	432	735	.615	1.085	3.55	3.85	698		*Sustained
	338	735	.460	.955	2.65	2.54	613		Intermittent
	345	735	.469	.955	2.71	2.59	609		*Intermittent
	311	830	.375	1.069	2.44	2.61	602		Sustained
	338	830	.407	.953	2.66	2.53	618		Sustained

*Top of flutter region.

TABLE II.- TABULATION OF FLUTTER DATA - Continued

$(\theta_{0.8R})_s$, deg	V_t, ft/sec	c, ft/sec	M_t	$\sqrt{\frac{\rho}{\rho_o}}$	$\frac{V_{0.8R}}{b\omega_\alpha}$	$\frac{V_{0.8R}}{b\omega_\alpha}\sqrt{\frac{\rho}{\rho_o}}$	ω_f, radians/sec	Mean $\Delta\theta_t$, deg	Characteristics of flutter
NACA 23018, blade 6(f) - continued									
20 ↓	404	830	0.487	0.953	3.17	3.03	625	0.4	*Sustained
	563	503	1.120	.869	4.42	3.84	---	↓	No flutter to V_t
	563	500	1.130	1.054	4.42	4.67	---		No flutter to V_t
22	267	1133	.236	.990	2.10	2.08	593	.1	Sustained
	348	1129	.308	.767	2.73	2.10	620		Intermittent
	360	1129	.319	.767	2.83	2.17	606		Sustained
	261	564	.463	1.073	2.05	2.20	583		Sustained
	282	564	.500	1.073	2.22	2.38	590		*Sustained
	235	670	.351	1.162	1.85	2.15	593		Sustained
	270	670	.403	1.019	2.12	2.16	595		Sustained
	362	670	.540	1.019	2.84	2.90	628		*Sustained
	261	800	.328	1.038	2.05	2.13	600		Sustained
	281	800	.353	.960	2.21	2.12	598		Sustained
	385	800	.484	.960	3.03	2.91	628		*Sustained
	563	494	1.140	.847	4.42	3.76	---		No flutter to V_t
↓	563	490	1.150	1.020	4.42	4.52	---	↓	No flutter to V_t
24	243	1117	.218	1.007	1.91	1.92	586	0	Sustained
	299	1118	.267	.850	2.35	2.00	616		Intermittent
	304	1118	.272	.850	2.39	2.03	604		Sustained
	241	572	.421	1.073	1.89	2.03	570		Sustained
	233	572	.407	1.073	1.83	1.97	576		Sustained
	253	580	.436	.979	1.99	1.95	570		Sustained
	249	580	.429	.979	1.96	1.92	570		Sustained
	234	583	.401	.979	1.84	1.80	576		Sustained
	245	583	.420	.979	1.93	1.89	570		*Sustained
	233	690	.338	1.085	1.83	1.99	576		Sustained
	263	690	.381	.944	2.07	1.95	583		Sustained
↓	296	690	.429	.944	2.33	2.20	586	↓	*Sustained

*Top of flutter region.

TABLE II.- TABULATION OF FLUTTER DATA - Continued

$(\theta_{0.8R})_s$, deg	V_t, ft/sec	c, ft/sec	M_t	$\sqrt{\frac{\rho}{\rho_0}}$	$\frac{V_{0.8R}}{b\omega_\alpha}$	$\frac{V_{0.8R}}{b\omega_\alpha}\sqrt{\frac{\rho}{\rho_0}}$	ω_T, radians/sec	Mean $\Delta\theta_t$, deg	Characteristics of flutter
NACA 23018, blade 6(f) - continued									
24	231	783	0.293	1.031	1.82	1.87	585	0	Sustained
↓	252	783	.322	.968	1.98	1.92	575	↓	Sustained
	377	783	.481	.968	2.96	2.87	614		*Sustained
	560	500	1.120	.906	4.40	3.99	---		No flutter to V_t
	560	500	1.120	1.015	4.40	4.47	---		No flutter to V_t
26	227	1130	.201	.994	1.78	1.77	581	0	Sustained
27	197	1120	.176	1.007	1.58	1.59	608	-.1	Sustained
↓	246	1120	.220	1.007	1.93	1.95	598	↓	Sustained
	230	580	.397	.992	1.81	1.79	576		Sustained
	259	580	.447	.992	2.03	2.02	572		*Sustained
	221	668	.331	.996	1.74	1.73	588		Sustained
	218	668	.326	.996	1.71	1.71	582		Sustained
	345	668	.517	.996	2.71	2.70	616		*Sustained
	222	754	.294	.998	1.74	1.74	568		Sustained
	211	824	.256	1.007	1.66	1.67	572		Intermittent
	222	824	.269	1.007	1.75	1.76	565		Sustained
	561	500	1.122	1.011	4.41	4.46	---		No flutter to V_t
28	225	1129	.199	.996	1.77	1.76	588	-.1	Sustained
30	441	502	.878	.944	3.47	3.27	---	-.5	No flutter to V_t
↓	441	500	.882	1.015	3.47	3.51	---	↓	No flutter to V_t
	441	584	.755	1.023	3.47	3.54	---		No flutter to V_t
	259	1129	.229	.996	2.04	2.03	588		Sustained
	258	644	.401	1.056	2.03	2.14	602		Sustained
	259	644	.402	1.005	2.04	2.05	608		Intermittent
	250	644	.388	1.005	1.97	1.97	608		*Intermittent
	262	723	.362	1.013	2.06	2.09	600		Intermittent
	287	723	.397	1.013	2.26	2.29	593		Sustained

*Top of flutter region.

TABLE II.- TABULATION OF FLUTTER DATA - Continued

$(\theta_{0.8R})_s$, deg	V_t, ft/sec	c, ft/sec	M_t	$\sqrt{\frac{\rho}{\rho_o}}$	$\frac{V_{0.8R}}{b\omega_\alpha}$	$\frac{V_{0.8R}}{b\omega_\alpha}\sqrt{\frac{\rho}{\rho_o}}$	ω_f, radians/sec	Mean $\Delta\theta_t$, deg	Characteristics of flutter
NACA 23018, blade 6(f) - concluded									
30	305	723	0.422	1.013	2.40	2.43	603	-0.5	*Sustained
↓	253	785	.322	1.009	1.99	2.01	614	↓	Intermittent
	291	785	.371	1.009	2.29	2.31	606		Sustained
	320	785	.408	1.009	2.52	2.54	603		*Sustained
	278	842	.330	.994	2.19	2.17	606		Sustained
NACA 23018, blade 6(r)									
11.3	525	1126	0.466	0.990	4.09	4.05	559	3.80	Sustained
↓	547	1128	.485	.924	4.27	3.93	571	↓	Sustained
	600	1129	.531	.872	4.67	4.07	581		Sustained
	541	1131	.478	.944	4.21	3.98	565		Sustained
	578	530	1.091	1.013	4.50	4.56	---		No flutter to V_t
	561	580	.967	1.058	4.37	4.62	---		No flutter to V_t
	407	625	.651	1.083	3.17	3.43	578		Sustained
	419	625	.670	1.083	3.26	3.54	590		*Sustained
	561	625	.898	1.040	4.37	4.54	---		No flutter to V_t
	425	658	.646	1.068	3.31	3.53	572		Sustained
	445	658	.676	1.068	3.47	3.70	600		*Sustained
	482	660	.730	1.005	3.75	3.77	---		No flutter to V_t
	441	685	.644	1.031	3.44	3.54	594		Sustained
	470	685	.686	1.031	3.66	3.77	612		*Sustained
	452	685	.660	.996	3.52	3.51	597		Sustained
	470	685	.686	.996	3.66	3.65	613		*Sustained
	458	685	.667	.957	3.57	3.41	606		Sustained
	463	685	.676	.957	3.61	3.45	616		*Sustained
	445	710	.627	.996	3.47	3.45	576		Sustained

*Top of flutter region.

TABLE II.- TABULATION OF FLUTTER DATA - Continued

$(\theta_{0.8R})_s$, deg	V_t, ft/sec	c, ft/sec	M_t	$\sqrt{\frac{\rho}{\rho_o}}$	$\frac{V_{0.8R}}{b\omega_\alpha}$	$\frac{V_{0.8R}}{b\omega_\alpha}\sqrt{\frac{\rho}{\rho_o}}$	ω_r, radians/sec	Mean $\Delta\theta_t$, deg	Characteristics of flutter
NACA 23018, blade 6(r) - continued									
11.3	490	710	0.690	0.996	3.82	3.80	619	3.80	*Sustained
↓	459	714	.643	.951	3.57	3.40	597	↓	Sustained
	485	714	.679	.951	3.78	3.60	622		*Sustained
	466	718	.649	.912	3.63	3.31	597		Sustained
	482	718	.671	.912	3.75	3.42	609		*Sustained
	463	720	.643	.875	3.61	3.15	597		Sustained
	482	720	.669	.875	3.75	3.28	---		*Sustained
	452	725	.623	.875	3.52	3.18	587		Sustained
	499	725	.688	.875	3.89	3.40	628		*Sustained
	474	725	.654	.805	3.69	2.97	590		Sustained
	448	785	.571	1.083	3.49	3.78	565		Sustained
	466	785	.594	1.013	3.63	3.68	575		Sustained
	494	785	.629	.901	3.85	3.47	594		Sustained
	499	785	.636	.789	3.89	3.07	597		Sustained
	510	910	.560	.996	3.97	3.96	584		Sustained
	516	910	.567	.942	4.02	3.79	584		Sustained
16.1	362	1097	.330	1.027	2.82	2.90	575	2.0	Sustained
↓	369	1098	.336	.975	2.87	2.80	578	↓	Sustained
	405	1098	.369	.894	3.15	2.82	590		Sustained
	438	1098	.399	.825	3.41	2.81	594		Sustained
	467	1098	.425	.748	3.64	2.72	600		Sustained
	285	485	.588	1.139	2.22	2.53	597		Sustained
	351	485	.724	1.139	2.73	3.11	628		*Sustained
	287	485	.592	1.066	3.01	2.39	597		Sustained
	294	485	.606	1.066	2.29	2.44	612		*Sustained
	302	485	.623	1.003	2.35	2.36	609		Intermittent

*Top of flutter region.

TABLE II.- TABULATION OF FLUTTER DATA - Continued

$(\theta_{0.8R})_s$, deg	V_t, ft/sec	c, ft/sec	M_t	$\sqrt{\frac{\rho}{\rho_o}}$	$\frac{V_{0.8R}}{b\omega_\alpha}$	$\frac{V_{0.8R}}{b\omega_\alpha}\sqrt{\frac{\rho}{\rho_o}}$	ω_r, radians/sec	Mean $\Delta\theta_t$, deg	Characteristics of flutter
NACA 23018, blade 6(r) - Continued									
16.1	562	487	1.154	0.935	4.38	4.09	---	2.0	No flutter to V_t
↓	353	620	.569	1.037	2.75	2.85	609	↓	Sustained
	429	620	.692	1.037	3.34	3.46	653		*Sustained
	351	628	.559	.960	2.73	2.63	616		Sustained
	380	628	.605	.960	2.96	2.84	616		*Sustained
	376	632	.595	.911	2.93	2.67	590		Intermittent
	552	635	.869	.865	4.30	3.72	---		No flutter to V_t
	364	750	.485	.995	2.83	2.82	565		Sustained
	362	760	.476	.939	2.82	2.65	565		Sustained
	386	762	.507	.884	3.00	2.66	584		Sustained
	483	762	.634	.884	3.76	3.33	628		Sustained
	408	762	.535	.822	3.18	2.61	584		Sustained
	487	762	.639	.822	3.79	3.12	622		*Sustained
	425	762	.558	.770	3.31	2.55	587		Sustained
	495	762	.650	.770	3.85	2.96	628		*Sustained
20.1	256	1098	.233	1.029	1.99	2.05	597	0.7	Sustained
↓	268	1096	.245	.979	2.09	2.04	603	↓	Sustained
	294	1096	.268	.899	2.29	2.05	603		Sustained
	321	1097	.293	.844	2.50	2.11	609		Sustained
	376	1097	.343	.775	2.93	2.27	603		Sustained
	386	1098	.352	.721	3.00	2.17	603		Sustained
	227	495	.459	1.025	1.77	1.81	597		Sustained
	256	495	.517	.943	1.99	1.88	603		Intermittent
	236	495	.477	1.051	1.84	1.93	597		Sustained
	311	495	.628	1.051	2.42	2.54	622		Sustained
	236	495	.477	.998	1.84	1.83	584		Sustained
	294	495	.593	.998	2.29	2.28	606		Sustained
	258	495	.520	.963	2.01	1.93	597		Sustained

*Top of flutter region.

TABLE II.- TABULATION OF FLUTTER DATA - Continued

$(\theta_{0.8R})_s$, deg	V_t, ft/sec	c, ft/sec	M_t	$\sqrt{\frac{\rho}{\rho_o}}$	$\frac{V_{0.8R}}{b\omega_\alpha}$	$\frac{V_{0.8R}}{b\omega_\alpha}\sqrt{\frac{\rho}{\rho_o}}$	ω_f, radians/sec	Mean $\Delta\theta_t$, deg	Characteristics of flutter
NACA 23018, blade 6(r) - continued									
20.1	272	495	0.550	0.963	2.12	2.04	612	0.7	*Sustained
	563	495	1.137	.905	4.38	3.97	---		No flutter to V_t
	284	615	.461	.938	2.21	2.07	609		Sustained
	339	615	.551	.938	2.64	2.48	615		*Sustained
	295	615	.480	.878	2.30	2.02	615		Intermittent
	557	630	.884	.833	4.34	3.61	---		No flutter to V_t
	232	627	.369	1.074	1.81	1.94	597		Sustained
	445	627	.710	1.074	3.46	3.72	676		*Sustained
	249	627	.397	1.018	1.94	1.98	584		Sustained
	436	627	.695	1.018	3.39	3.45	597		*Sustained
	261	627	.416	.970	2.03	1.98	581		Sustained
	425	627	.678	.970	3.31	3.21	641		*Sustained
	281	627	.448	.935	2.19	2.04	597		Sustained
	397	627	.633	.935	3.09	2.89	625		*Sustained
	285	627	.455	.894	2.22	1.99	597		Sustained
	342	627	.546	.894	2.66	2.38	609		*Sustained
	292	627	.466	.882	2.27	2.01	597		Sustained
	330	627	.526	.882	2.57	2.27	603		*Sustained
	297	627	.474	.863	2.31	2.00	590		Sustained
	312	627	.498	.863	2.43	2.09	610		*Sustained
	289	627	.461	.842	2.25	1.90	603		Intermittent
	268	770	.348	.978	2.09	2.05	581		Sustained
	281	770	.365	.943	2.19	2.06	590		Sustained
	301	770	.391	.891	2.35	2.09	590		Sustained
	336	770	.436	.807	2.62	2.11	603		Sustained
	565	770	.734	.750	4.40	3.30	---		No flutter to V_t
	432	1106	.391	.672	3.37	2.26	581		Sustained
	482	1106	.436	.651	3.76	2.45	597		Sustained

*Top of flutter region.

TABLE II.- TABULATION OF FLUTTER DATA - Continued

$(\theta_{0.8R})_B$, deg	V_t, ft/sec	c, ft/sec	M_t	$\sqrt{\frac{\rho}{\rho_o}}$	$\frac{V_{0.8R}}{b\omega_\alpha}$	$\frac{V_{0.8R}}{b\omega_\alpha}\sqrt{\frac{\rho}{\rho_o}}$	ω_f, radians/sec	Mean $\Delta\theta_t$, deg	Characteristics of flutter
NACA 23018, blade 6(r) - continued									
23.4	252	1112	0.227	1.013	1.96	1.99	572	0	Sustained
	268	1112	.241	.944	2.09	1.97	565		Sustained
	273	1112	.246	.889	2.13	1.89	572		Sustained
	295	1112	.265	.831	2.30	1.91	578		Sustained
	359	1112	.323	.752	2.80	2.10	578		Sustained
	429	1112	.386	.695	3.34	2.33	587		Sustained
	579	1115	.519	.645	4.51	2.91	612		Sustained
	305	497	.614	.999	2.38	2.38	597		*Intermittent
	223	497	.449	.999	1.74	1.73	565		Intermittent
	341	497	.686	1.026	2.66	2.73	609		*Intermittent
	220	497	.443	1.026	1.71	1.76	572		Intermittent
	327	497	.658	1.056	2.55	2.69	590		*Intermittent
	263	497	.529	1.056	2.05	2.16	603		Intermittent
	336	497	.676	1.087	2.62	2.85	609		*Intermittent
	235	497	.473	1.087	1.83	1.99	585		Intermittent
	214	497	.431	1.116	1.67	1.86	581		Intermittent
	341	497	.686	1.116	2.65	2.96	622		*Intermittent
	254	560	.454	.996	1.98	1.97	559		Sustained
	351	560	.627	.996	2.73	2.72	609		*Sustained
	254	562	.452	.954	1.98	1.89	559		Sustained
	349	562	.621	.954	2.72	2.59	597		*Sustained
	251	563	.446	.913	1.96	1.78	559		Sustained
	341	563	.606	.913	2.66	2.43	590		*Sustained
	563	565	.997	.847	4.38	3.71	---		No flutter to V_t
	337	570	.591	.876	2.63	2.30	590		*Sustained
	268	570	.470	.876	2.09	1.83	562		Sustained

*Top of flutter region.

TABLE II.- TABULATION OF FLUTTER DATA - Continued

$(\theta_{0.8R})_s$, deg	V_t, ft/sec	c, ft/sec	M_t	$\sqrt{\rho/\rho_o}$	$\frac{V_{0.8R}}{b\omega_\alpha}$	$\frac{V_{0.8R}}{b\omega_\alpha}\sqrt{\rho/\rho_o}$	ω_f, radians/sec	Mean $\Delta\theta_t$, deg	Characteristics of flutter
NACA 23018, blade 6(r) - concluded									
23.4	254	660	0.385	0.933	1.98	1.85	559	0	Sustained
	423	660	.641	.933	3.30	3.07	635		*Sustained
	271	660	.411	.881	2.11	1.86	565		Sustained
	397	660	.602	.881	3.09	2.73	603		Sustained
	565	660	.856	.821	4.40	3.61	---		No flutter to V_t
	298	660	.452	.850	2.32	1.97	572		Sustained
	396	660	.600	.850	3.09	2.62	597		Sustained
	255	763	.334	.922	1.99	1.83	553		Sustained
	281	763	.368	.866	2.19	1.90	553		Sustained
	486	763	.637	.866	3.79	3.27	635		Sustained
	313	763	.410	.807	2.44	1.97	553		Intermittent
	389	763	.510	.807	3.03	2.44	573		Intermittent
	386	763	.506	.791	3.01	2.35	581		Intermittent
	310	763	.406	.791	2.42	1.91	565		Intermittent
	565	763	.741	.771	4.40	3.39	---		No flutter to V_t

*Top of flutter region.

TABLE II.- TABULATION OF FLUTTER DATA - Concluded

$(\theta_{0.8R})_s$, deg	V_t, ft/sec	c, ft/sec	M_t	$\sqrt{\frac{\rho}{\rho_0}}$	$\frac{V_{0.8R}}{b\omega_\alpha}$	$\frac{V_{0.8R}}{b\omega_\alpha}\sqrt{\frac{\rho}{\rho_0}}$	ω_f, radians/sec	Mean $\Delta\theta_t$, deg	Characteristics of flutter
NACA 23018, blade 7(r)									
11.0	508	1130	0.450	0.997	4.74	4.72	538	2.3	Intermittent
13.0	402	1129	.356	.997	3.75	3.74	524	2.1	Sustained
15.0	353	1130	.312	.995	3.30	3.28	523	1.6	Sustained
17.0	283	1131	.250	.995	2.64	2.63	514	1.3	Sustained
19.3	231	1132	.204	.993	2.16	2.14	516	.5	Sustained
22.3	214	1132	.189	.993	2.00	1.99	502	.1	Sustained
25.0	241	1128	.214	.997	2.25	2.24	502	0	Sustained
NACA 23018, blade 8(r)									
13.0	444	1119	0.397	1.005	3.70	3.72	579	3.2	Sustained
15.0	365	1127	.324	.997	3.04	3.03	565	2.3	Sustained
17.0	308	1126	.274	.998	2.57	2.56	570	1.5	Sustained
19.3	252	1122	.225	1.002	2.10	2.11	576	.8	Sustained
22.0	250	1122	.223	1.002	2.08	2.09	566	.2	Sustained
25.8	275	1122	.245	1.002	2.29	2.30	593	0	Intermittent
NACA 23018, blade 9(r)									
13.0	452	1119	0.405	1.005	3.86	3.88	565	3.2	Sustained
15.0	421	1127	.373	.997	3.60	3.59	575	2.3	Sustained
17.0	351	1126	.312	.998	3.00	2.99	557	1.5	Sustained
19.3	301	1122	.268	1.002	2.57	2.58	542	.8	Sustained
22.0	276	1122	.246	1.002	2.36	2.37	534	.2	Sustained
25.8	337	1122	.300	1.002	2.88	2.89	530	0	Sustained

TABLE III.- EFFECT OF MACH NUMBER AND DIVERGENCE ON BLADE TWIST

[NACA 23012 blade 4(r); $(\theta_{0.8R})_s = 5^\circ$; atmospheric density]

c	V_t	M_t	$\frac{V_{0.8R}}{b\omega_\alpha}\sqrt{\frac{\rho}{\rho_o}}$	$\Delta\theta_t$	$\frac{\Delta\theta_t}{\frac{V_{0.8R}}{b\omega_\alpha}\sqrt{\frac{\rho}{\rho_o}}}$
500	160	0.32	1.83	0.5	0.27
	240	.48	2.74	1.3	.47
	320	.64	3.65	3.1	.85
	360	.72	4.11	4.1	1.00
	400	.80	4.57	4.4	.96
	440	.88	5.03	4.4	.88
	480	.96	5.49	4.0	.73
565	160	.28	1.83	1.1	.60
	240	.43	2.74	1.9	.69
	320	.57	3.65	3.1	.85
	360	.64	4.11	4.3	1.05
	400	.71	4.57	6.1	1.34
602	160	.27	1.83	1.0	.55
	240	.40	2.74	1.8	.66
	320	.53	3.65	2.8	.77
	360	.60	4.11	3.3	.80
	400	.67	4.57	5.6	1.23
	400	.67	[a]4.01	4.0	[a]1.00
	440	.73	5.03	6.2	1.23
	440	.73	[a]4.41	4.9	[a]1.11
	480	.80	[a]4.80	4.9	[a]1.02
715	160	.22	1.83	.7	.38
	240	.34	2.74	1.2	.44
	320	.45	3.65	1.9	.52
	400	.56	4.57	5.2	1.14
	420	.59	4.80	7.0	1.46
1120	160	.14	1.83	.8	.44
	320	.28	3.65	1.9	.52
	400	.36	4.57	5.2	1.14
	480	.43	5.49	9.5	1.73

[a]Density reduced to 0.77 atmosphere.

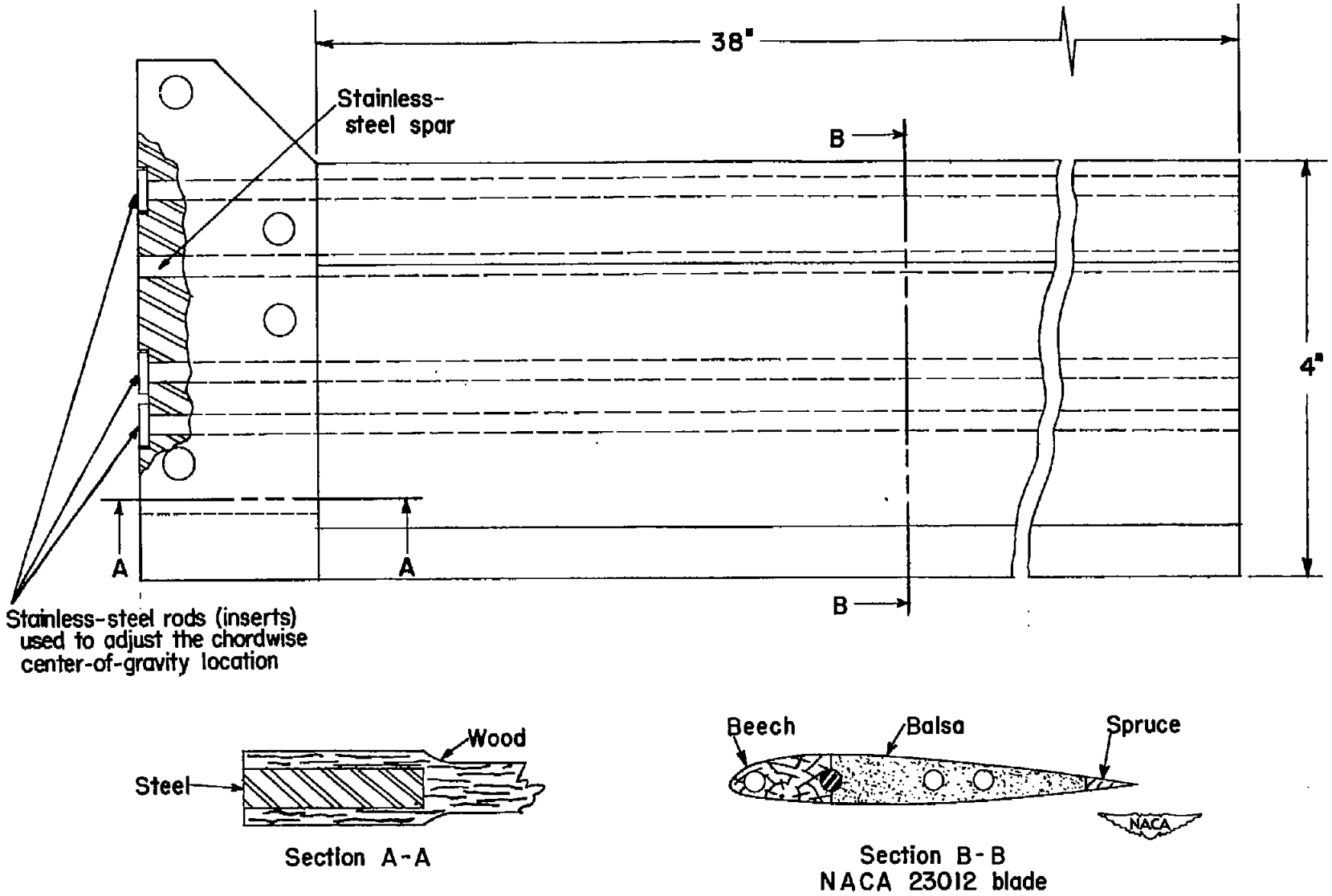

Figure 1.- Schematic drawing of blade showing method of varying chordwise center-of-gravity location.

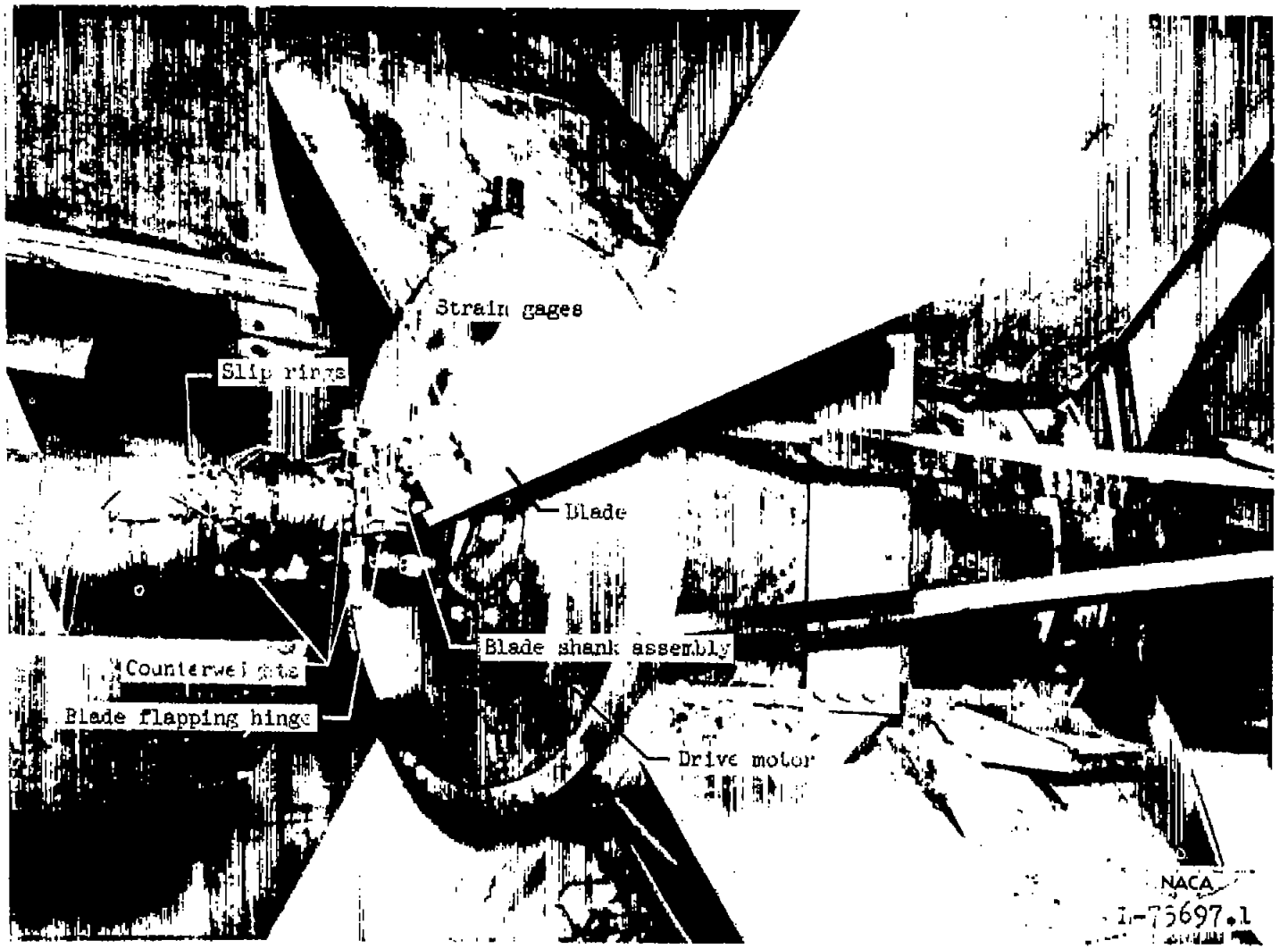

Figure 2.- Rotor-blade assembly as viewed with the hub mounted on the motor shaft inside the vacuum sphere.

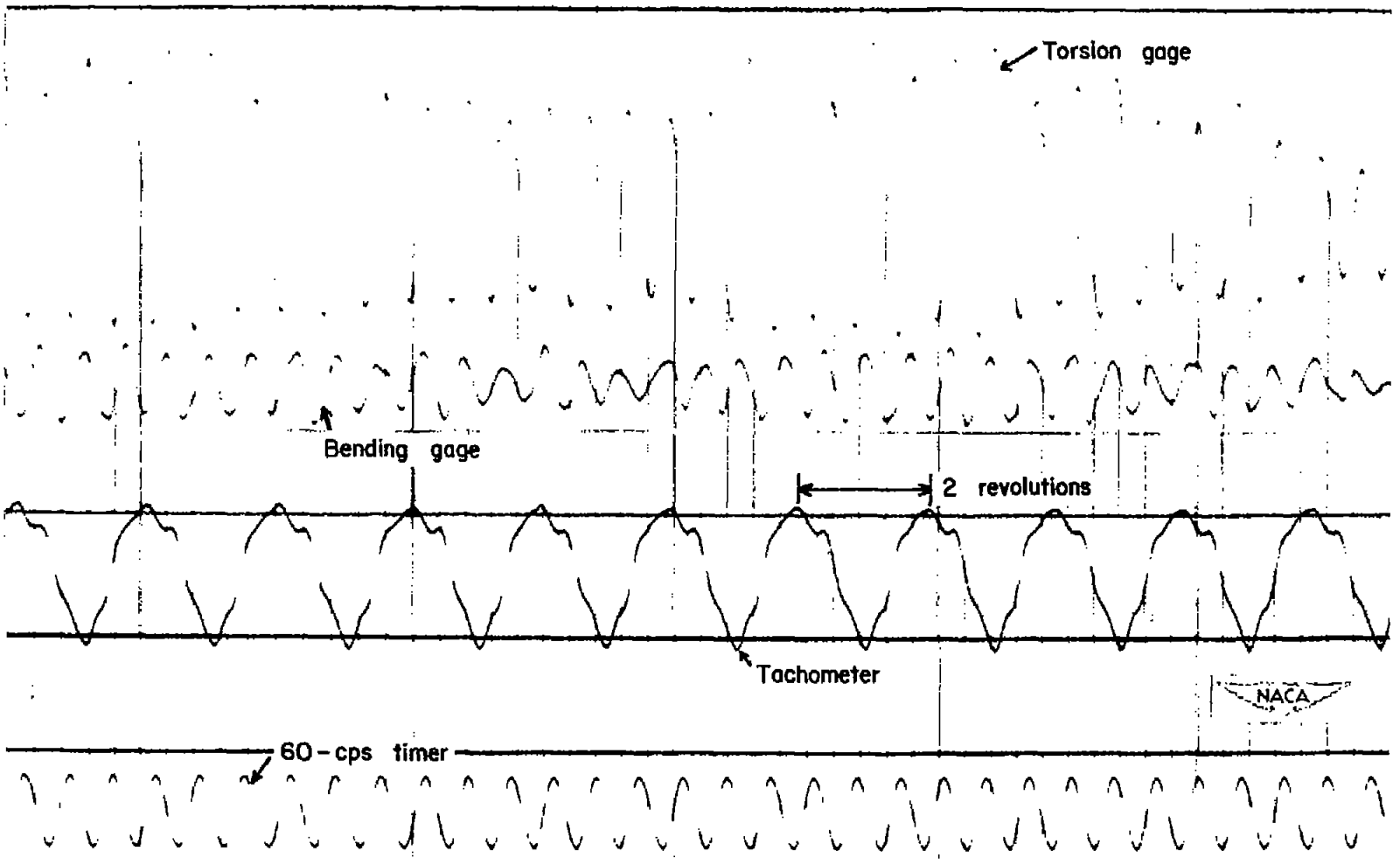

Figure 3.- Sample flutter record.

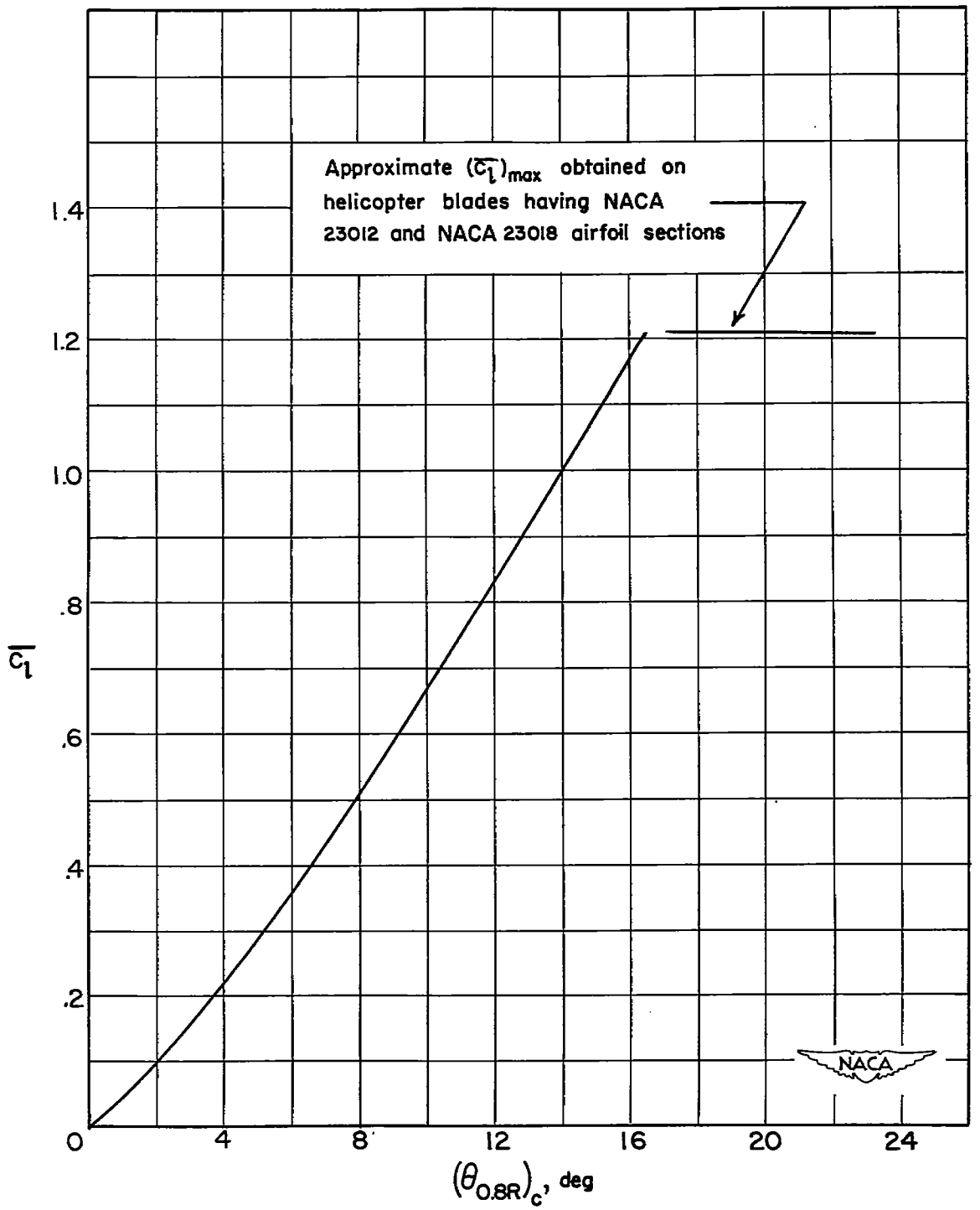

Figure 4.- Mean section lift coefficient for the NACA 23012 and 23018 blades as a function of the blade pitch angle. (The lift coefficient is calculated by Glauert's method, ref. 6, based on a blade element located at 0.8R.) $\sigma = 0.028$.

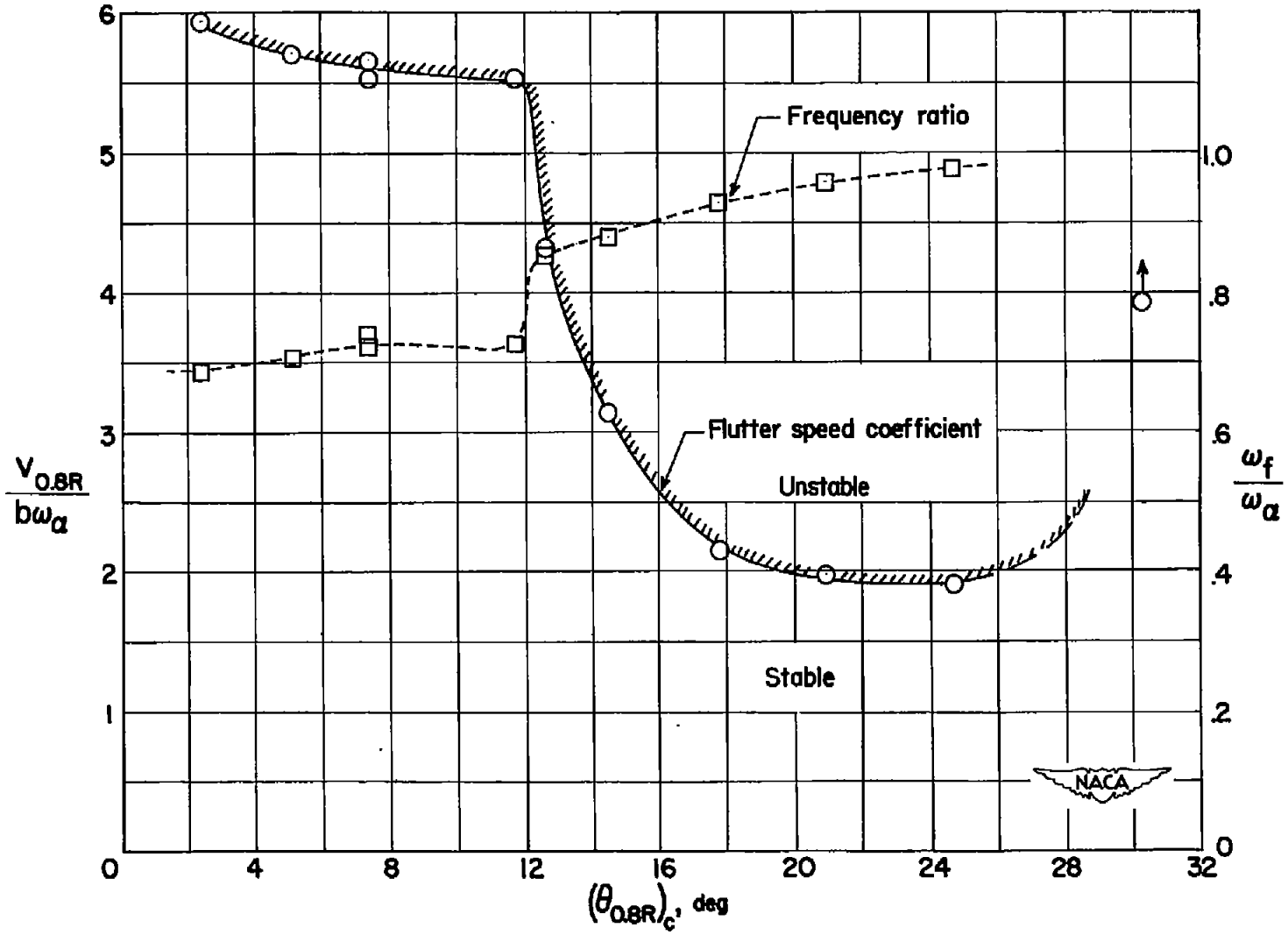

Figure 5.- The variation of flutter speed coefficient and flutter frequency ratio with blade pitch angle for blade 1(r) at atmospheric density. $M_t < 0.51$.

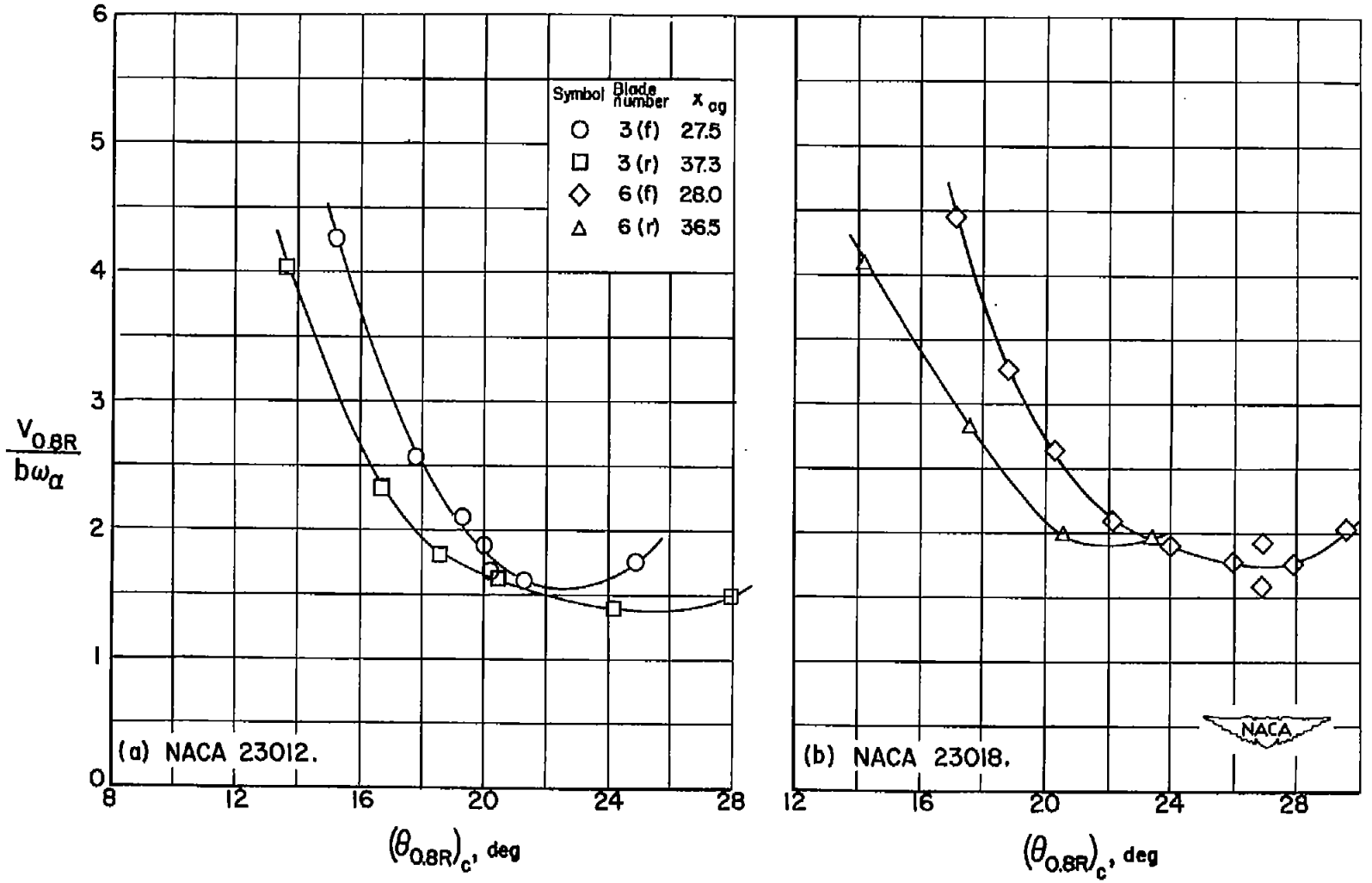

Figure 6.- The effect of chordwise center-of-gravity location on the flutter speed coefficient as a function of blade pitch angle at atmospheric density for blades having both NACA 23012 and NACA 23018 airfoil sections. $M_t < 0.51$.

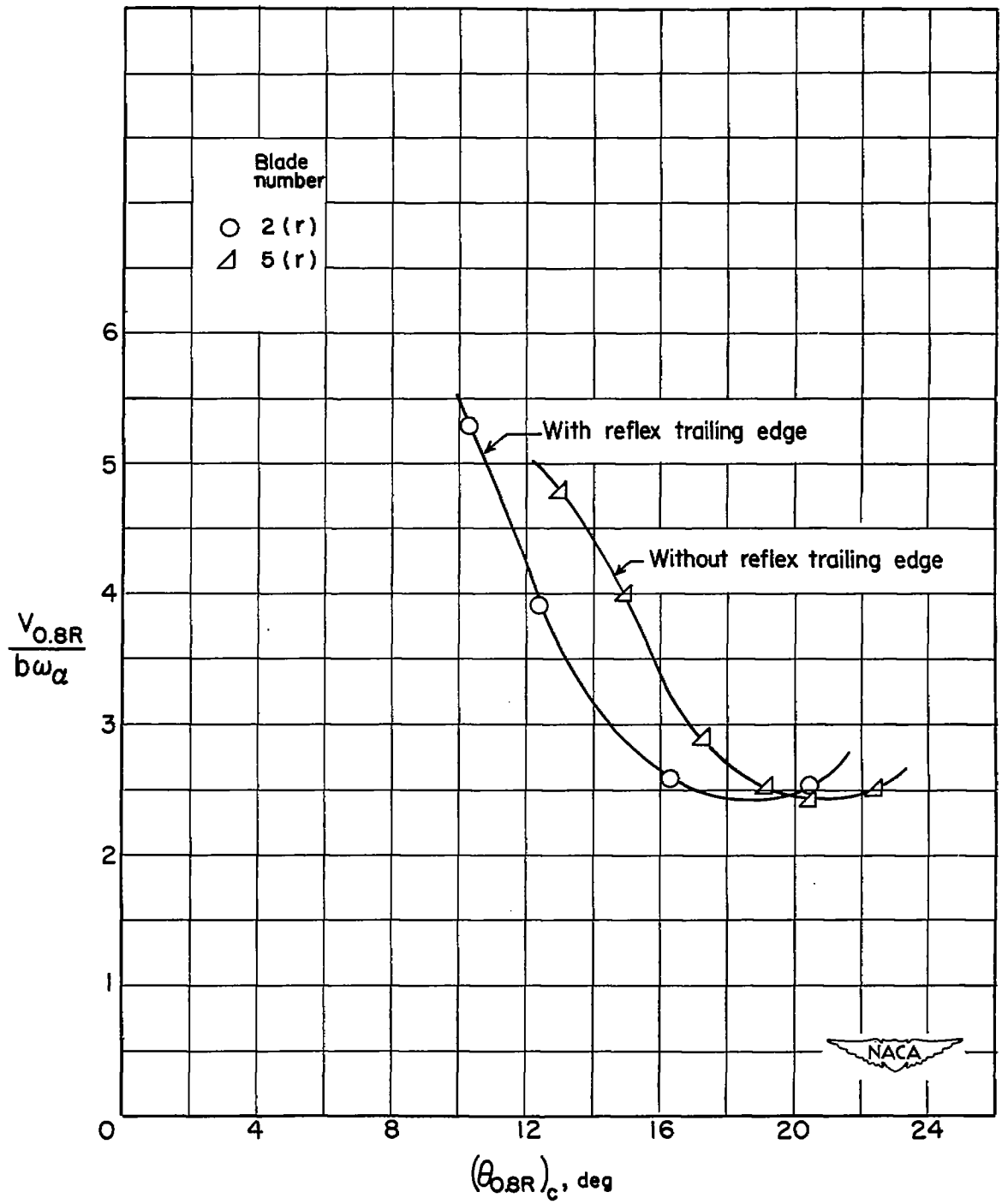

Figure 7.- The effect of blade airfoil shape on the flutter speed coefficient as a function of blade pitch angle at atmospheric densities. $M_t < 0.44$.

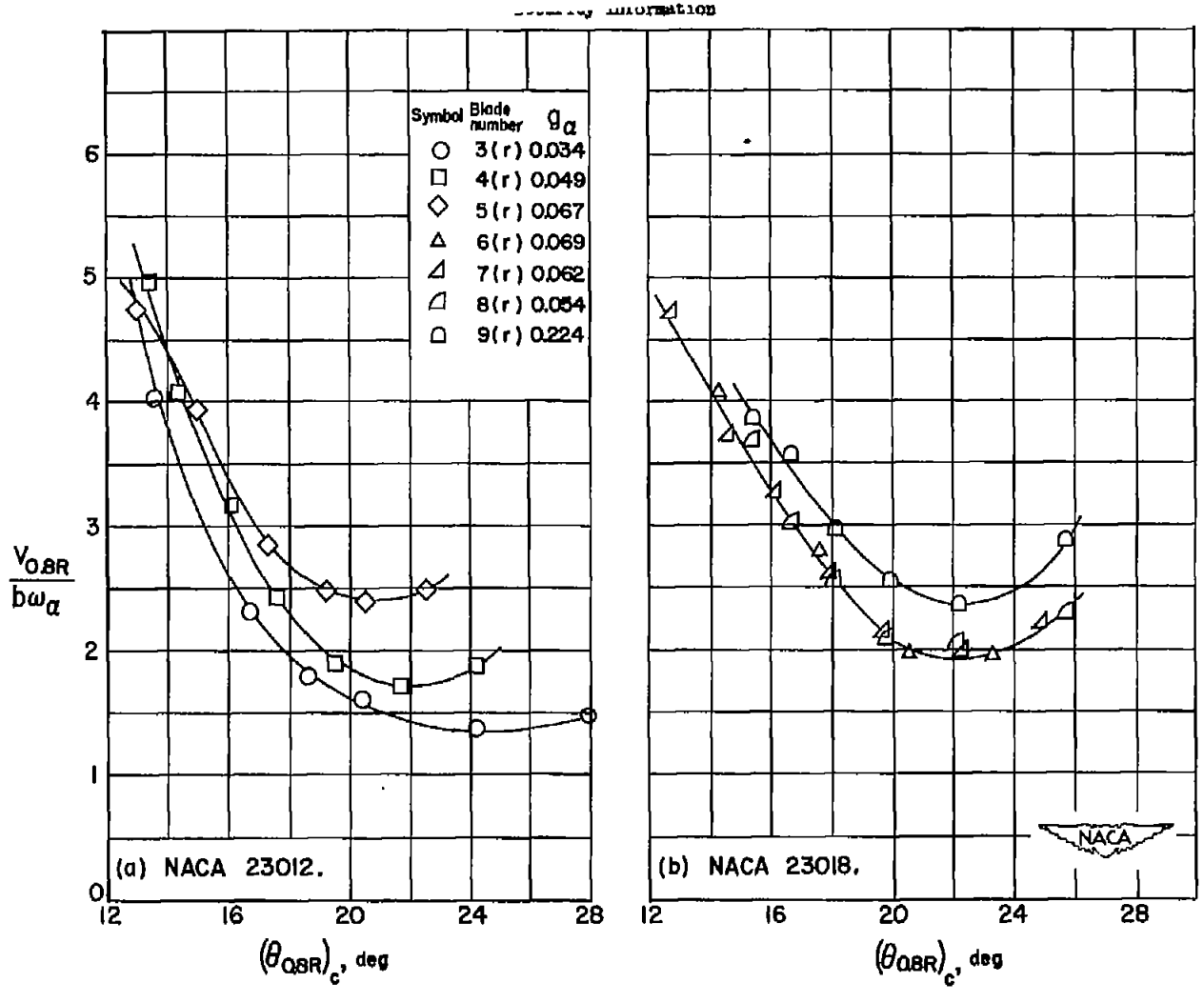

Figure 8.- The effect of structural damping on the flutter speed coefficient as a function of blade pitch angle at atmospheric density for blades having both NACA 23012 and NACA 23018 airfoil sections. $M_t < 0.43$.

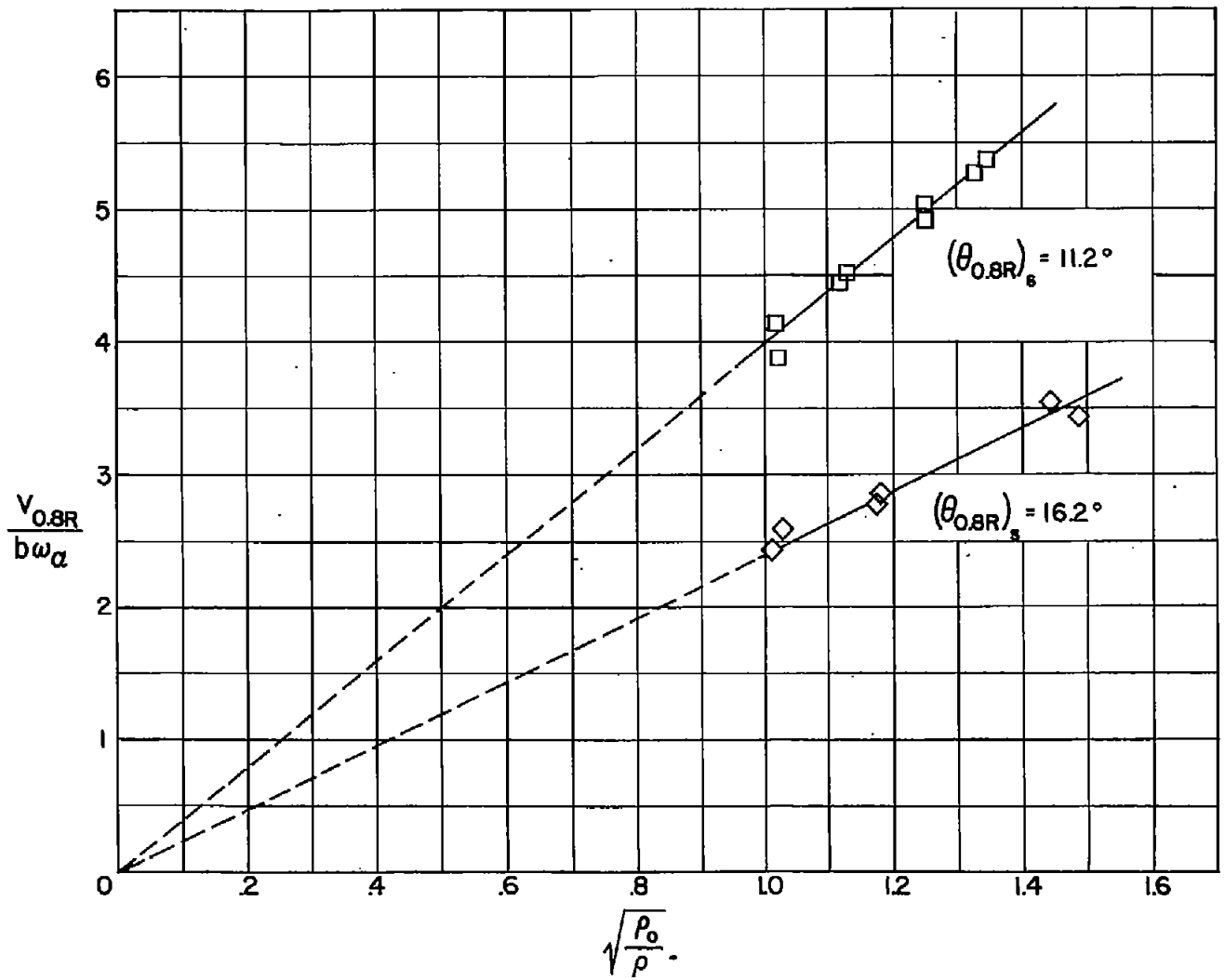

Figure 9.- The effect of density on the flutter speed coefficient at medium and high pitch angles for blade number 2(r). $M_t < 0.42$.

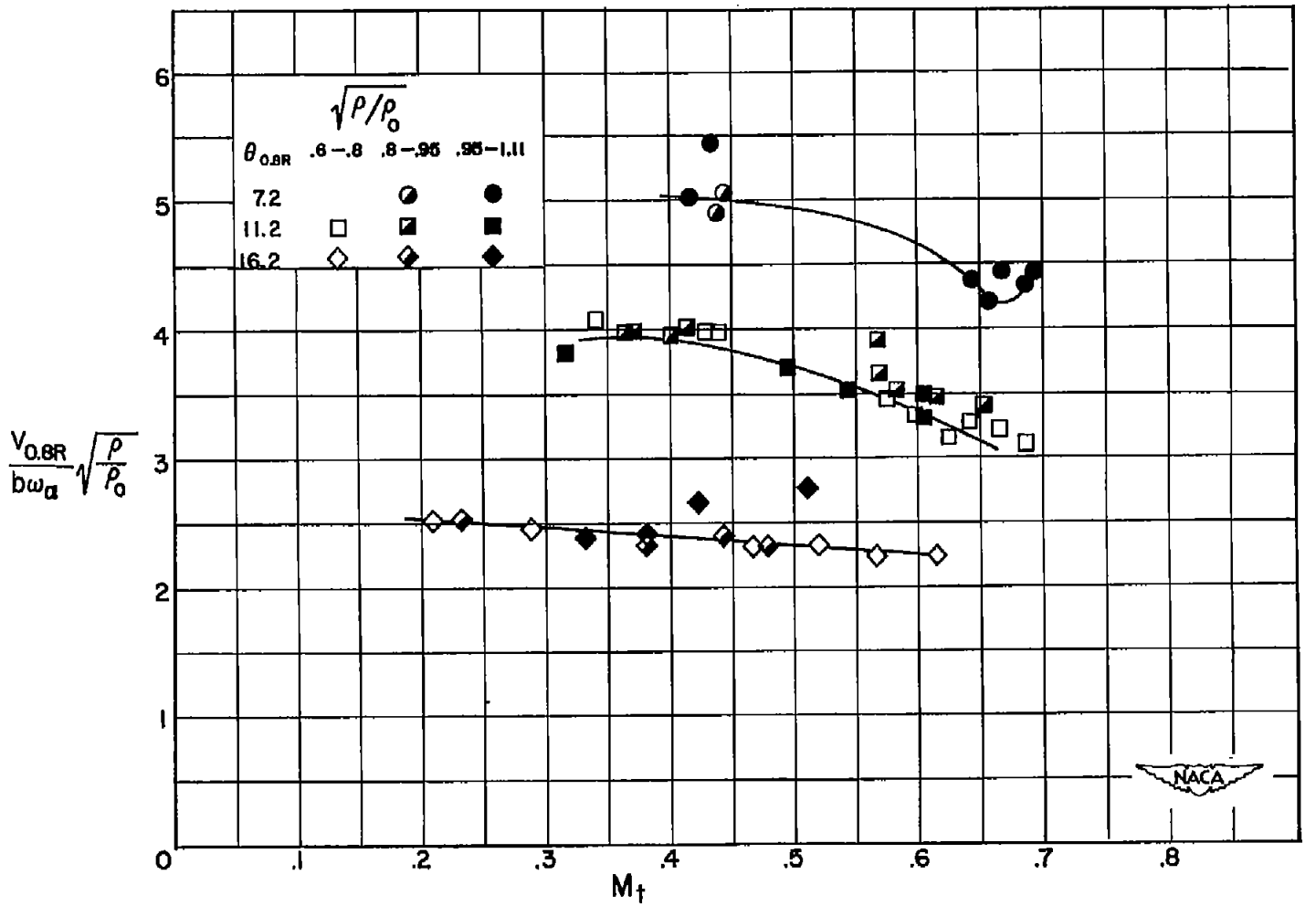

Figure 10.- The modified flutter speed coefficient as a function of tip Mach number at various pitch angles. (Data are presented for different density ratios to show that the flutter boundaries are not altered by changes in density when the flutter speed coefficient is modified by the square root of the density ratio.)

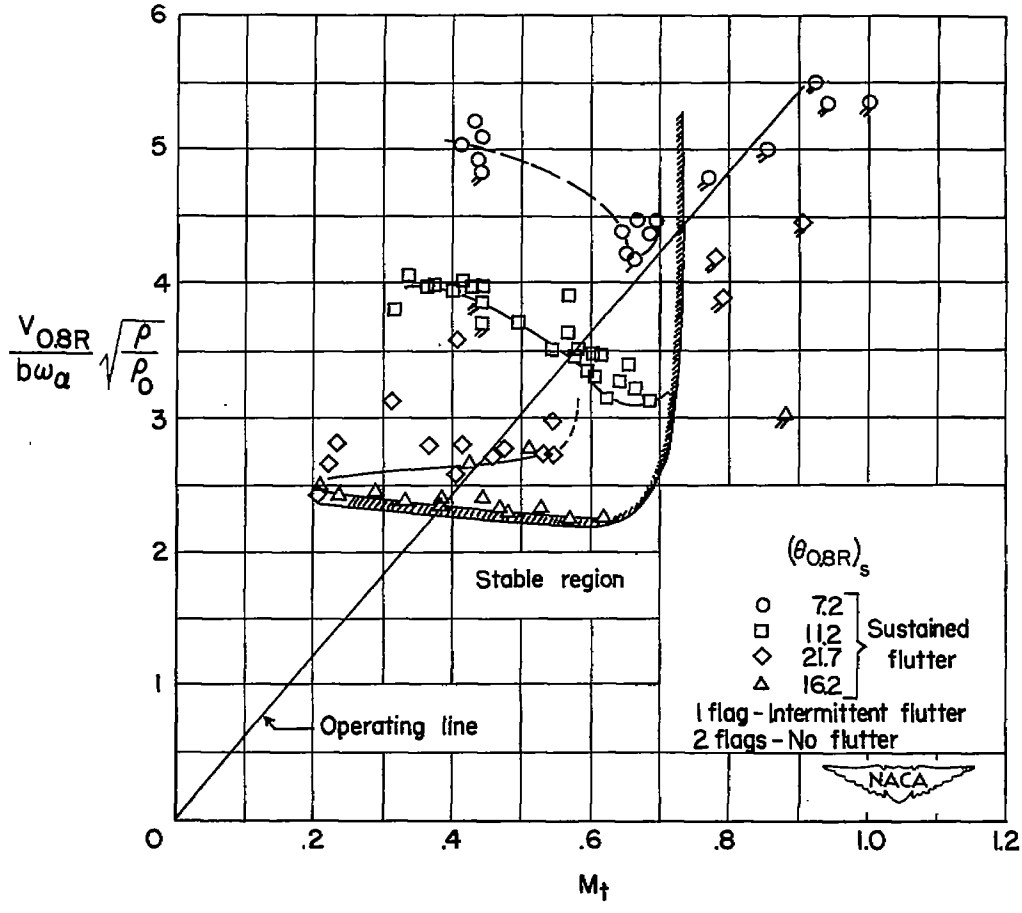

(a) Blade number 2(r); $g_\alpha = 0.075$.

Figure 11.- The effect of tip Mach number on the modified flutter speed coefficient at various pitch-angle settings for two blades having NACA 23012 airfoil sections.

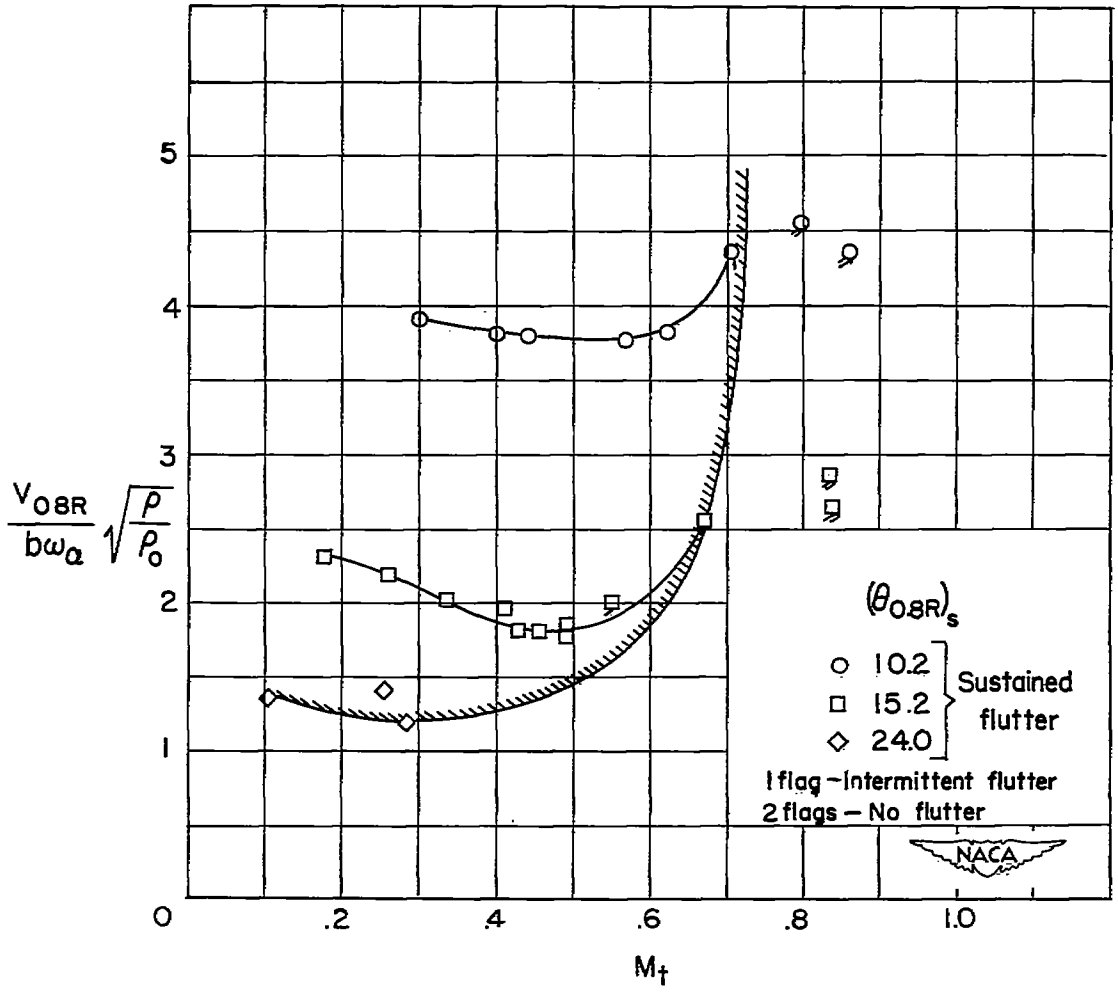

(b) Blade number 3(r); $g_\alpha = 0.034$.

Figure 11.- Concluded.

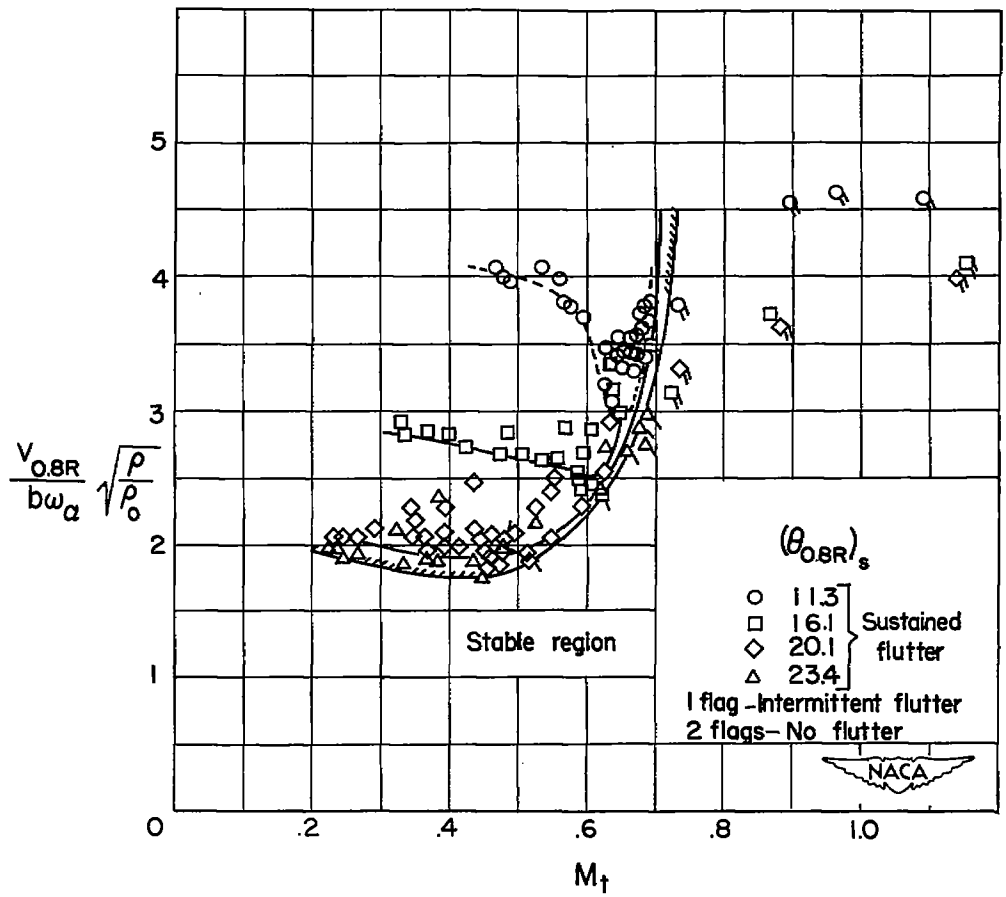

(a) Blade number 6(r); $g_\alpha = 0.069$.

Figure 12.- The effect of tip Mach number on the modified flutter speed coefficient at various pitch-angle settings for a blade having an NACA 23018 airfoil section at different chordwise center-of-gravity locations.

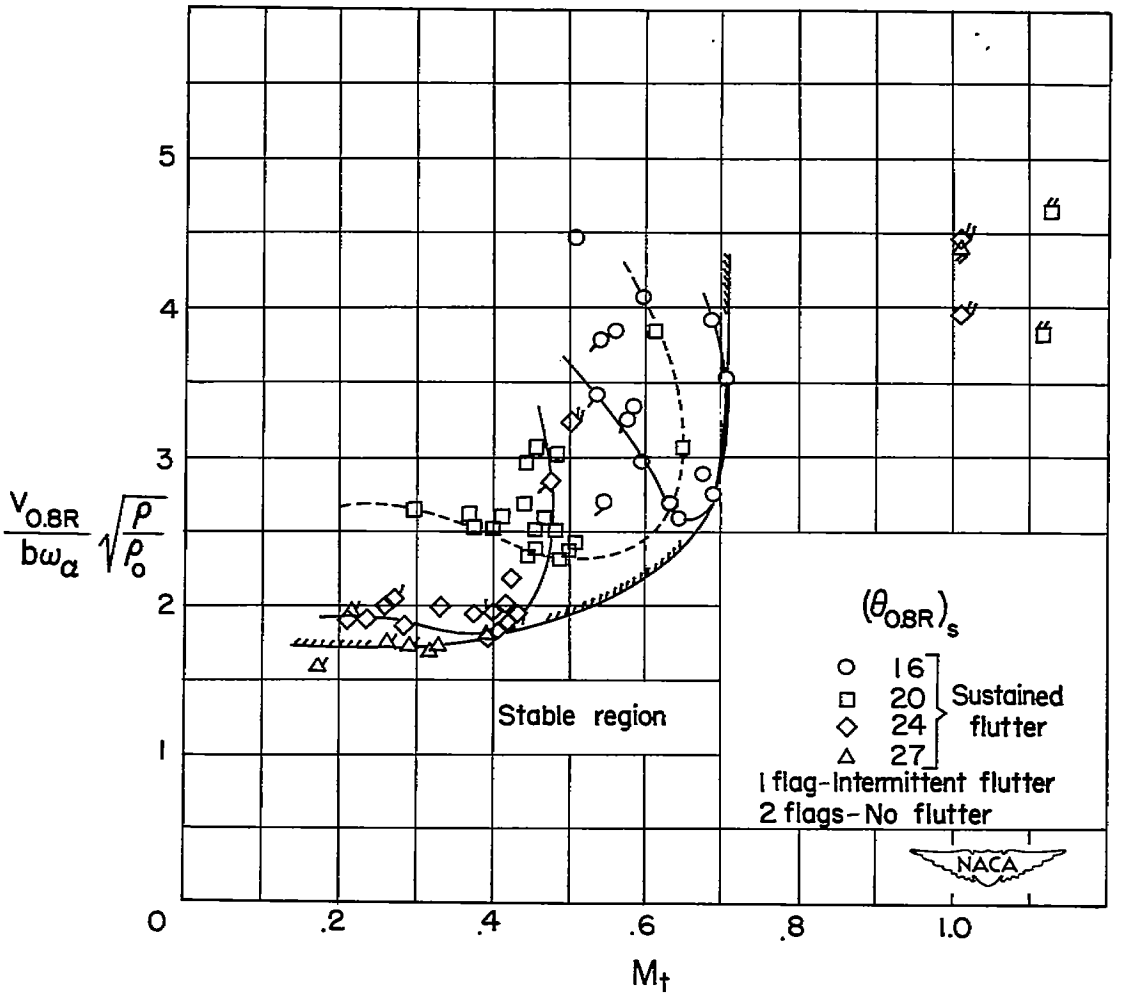

(b) Blade number 6(f); $g_\alpha = 0.064$.

Figure 12.- Concluded.

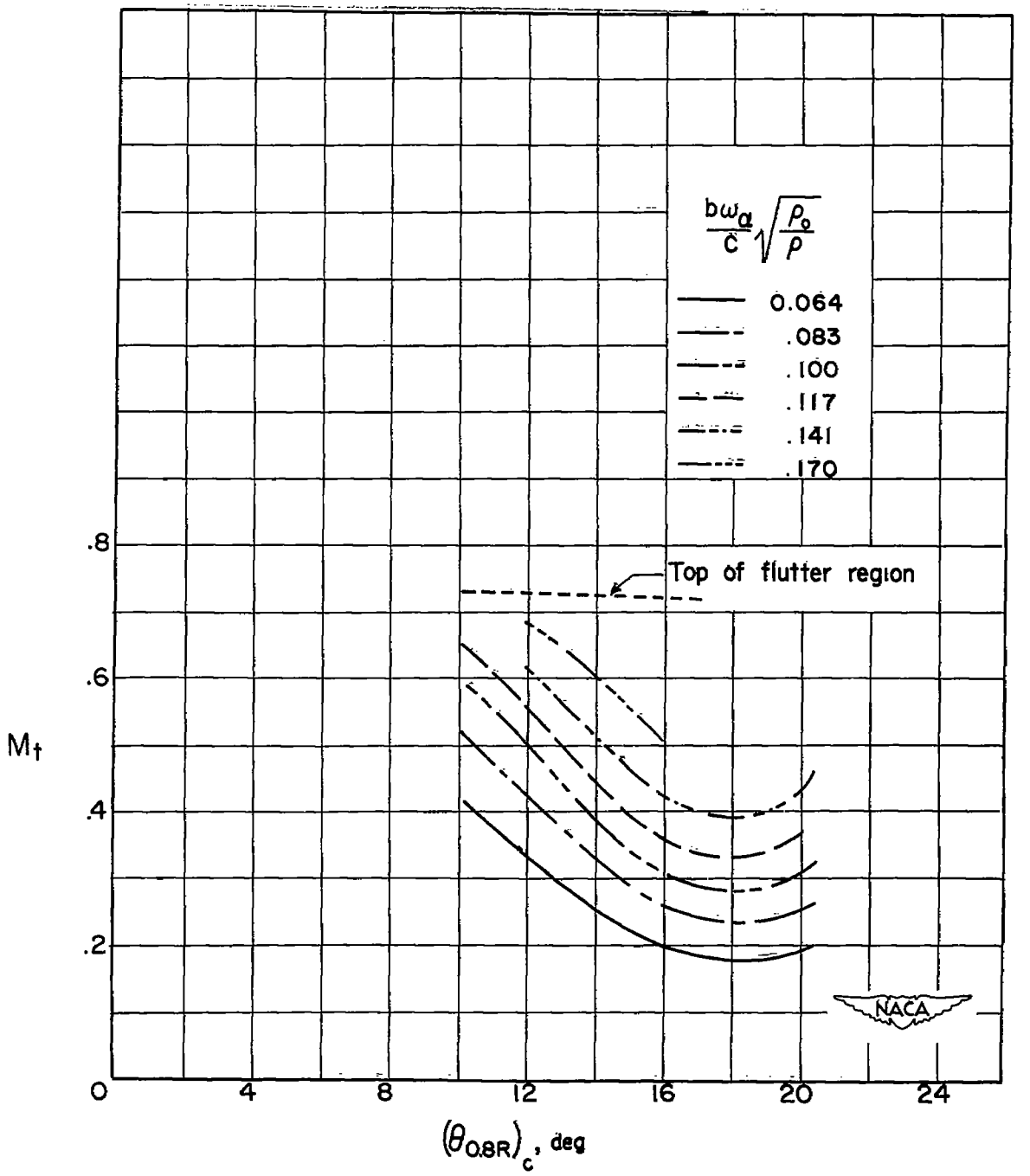

Figure 13.- The effect of blade pitch angle (corrected for twist) on the tip Mach number at flutter for various values of the dimensionless flutter parameter $\frac{b\omega_\alpha}{c}\sqrt{\frac{\rho_0}{\rho}}$ for blade 2(r).

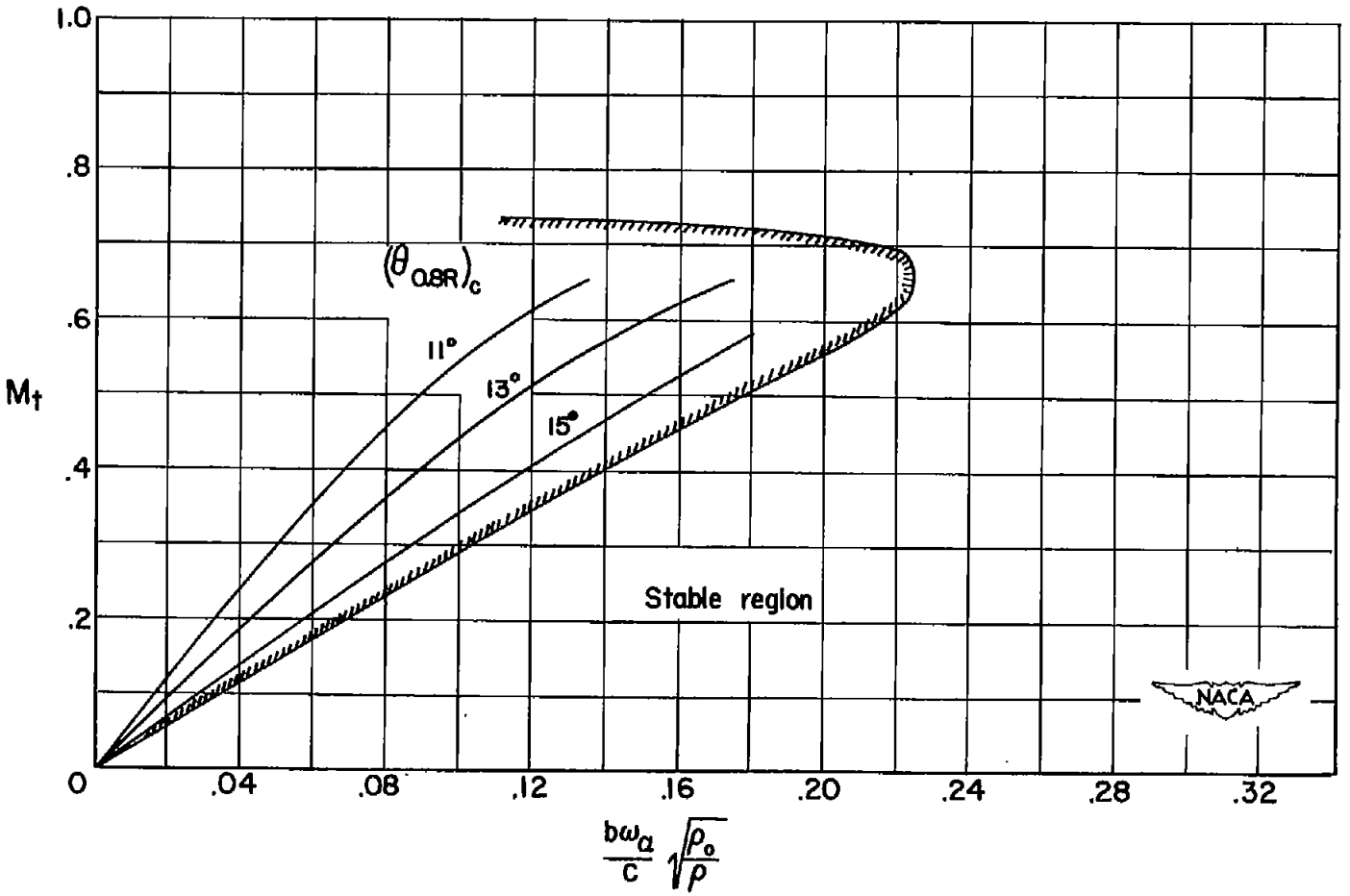

Figure 14.- The effect of the flutter parameter on the tip Mach number at flutter at various pitch angles for blade 2(r).

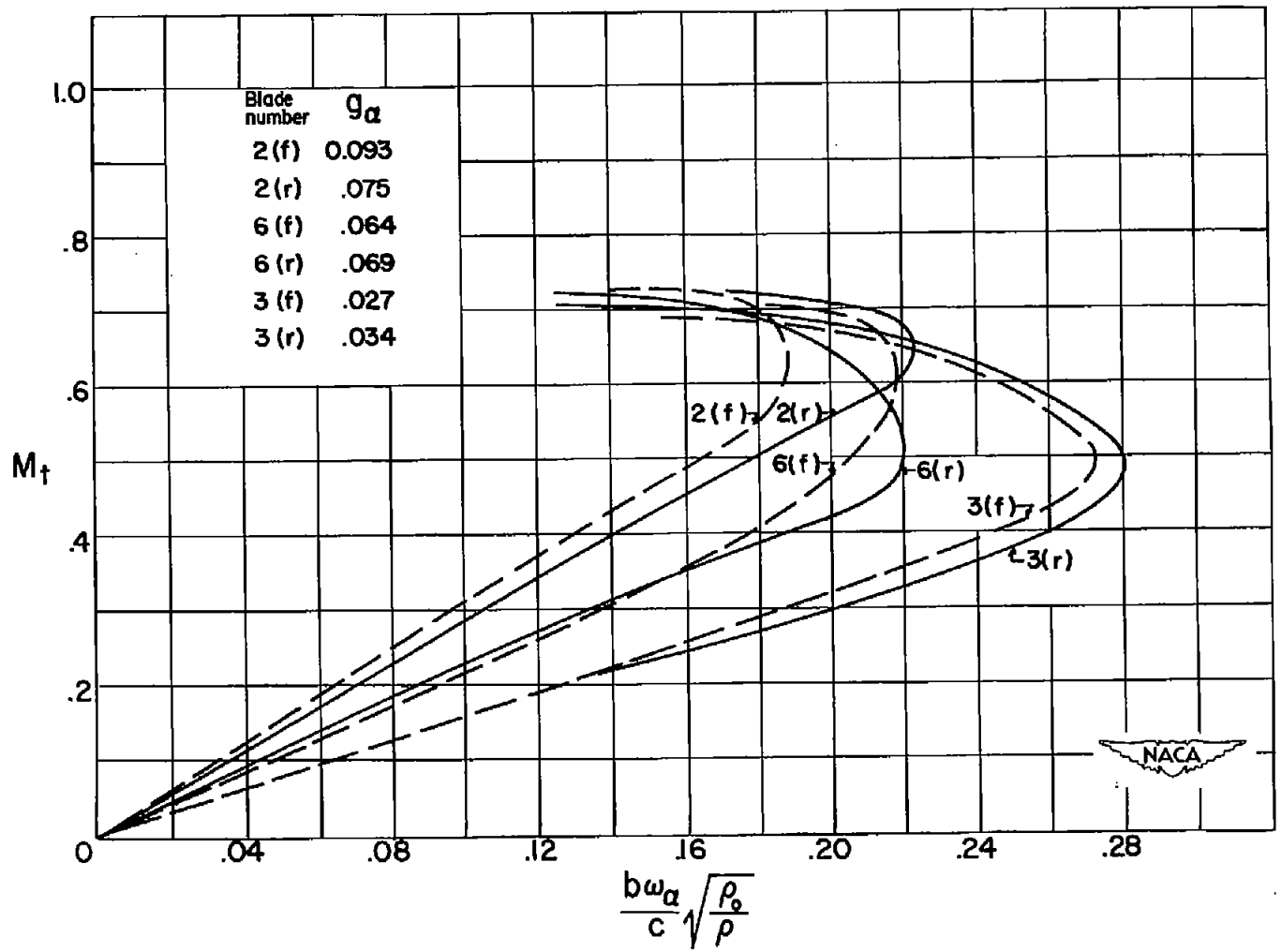

Figure 15.- The envelope flutter boundaries plotted in terms of the tip Mach number and flutter parameter for various blades having different airfoil sections, chordwise center-of-gravity locations, and structural damping coefficients.

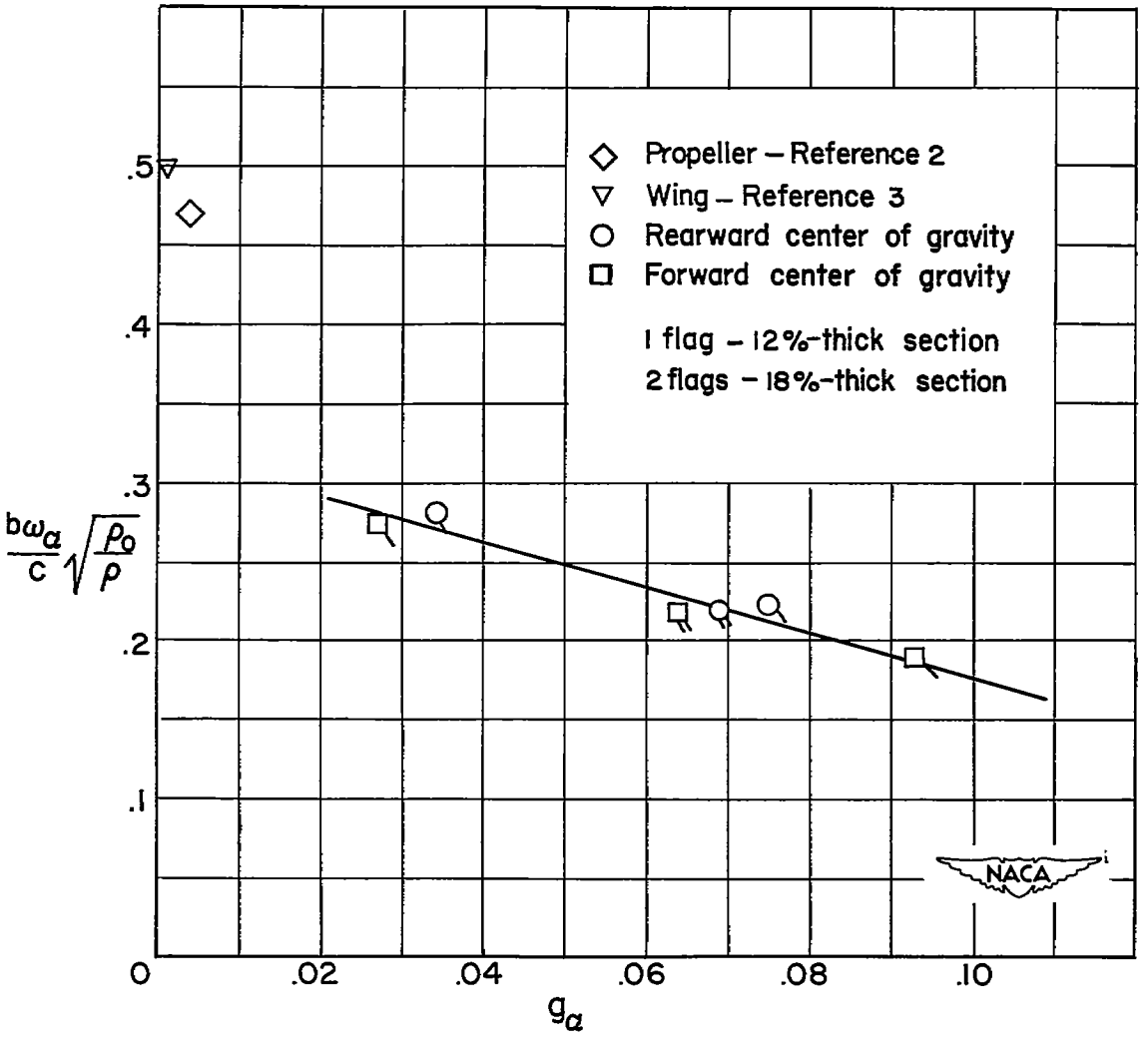

Figure 16.- The variation of critical values of the design flutter parameter with torsional damping.

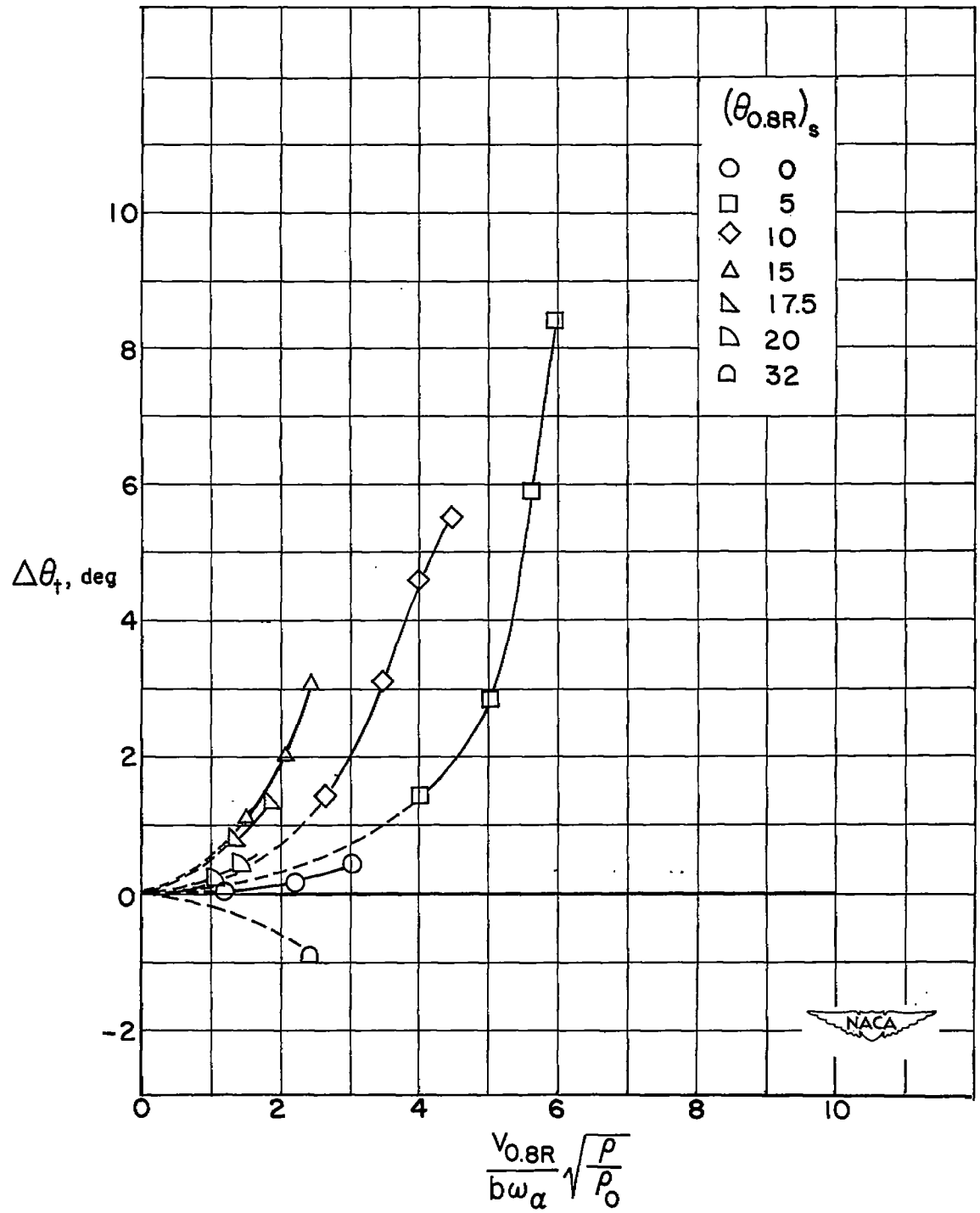

Figure 17.- Measured twist as a function of flutter speed coefficient at various pitch-angle settings for blade 3(r). $M_t < 0.43$.

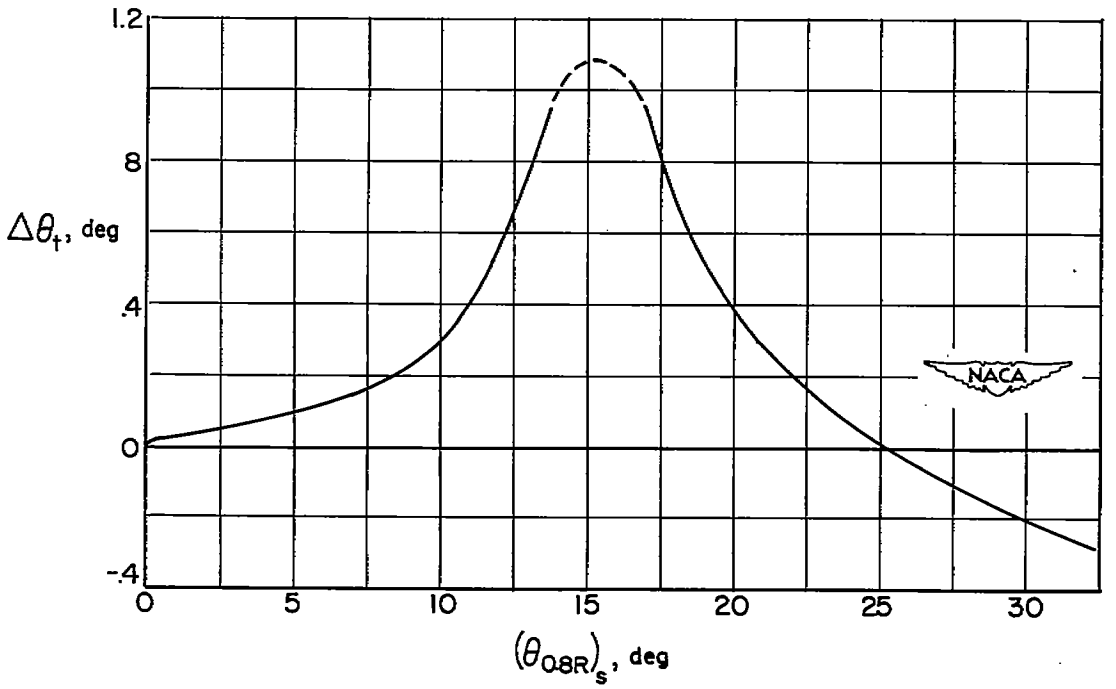

Figure 18.- Measured twist as a function of pitch-angle setting for blade 3(r). Data taken from figure 17 for $(V_{0.8R}/b\omega\alpha)(\sqrt{\rho/\rho_0}) = 1.4$.

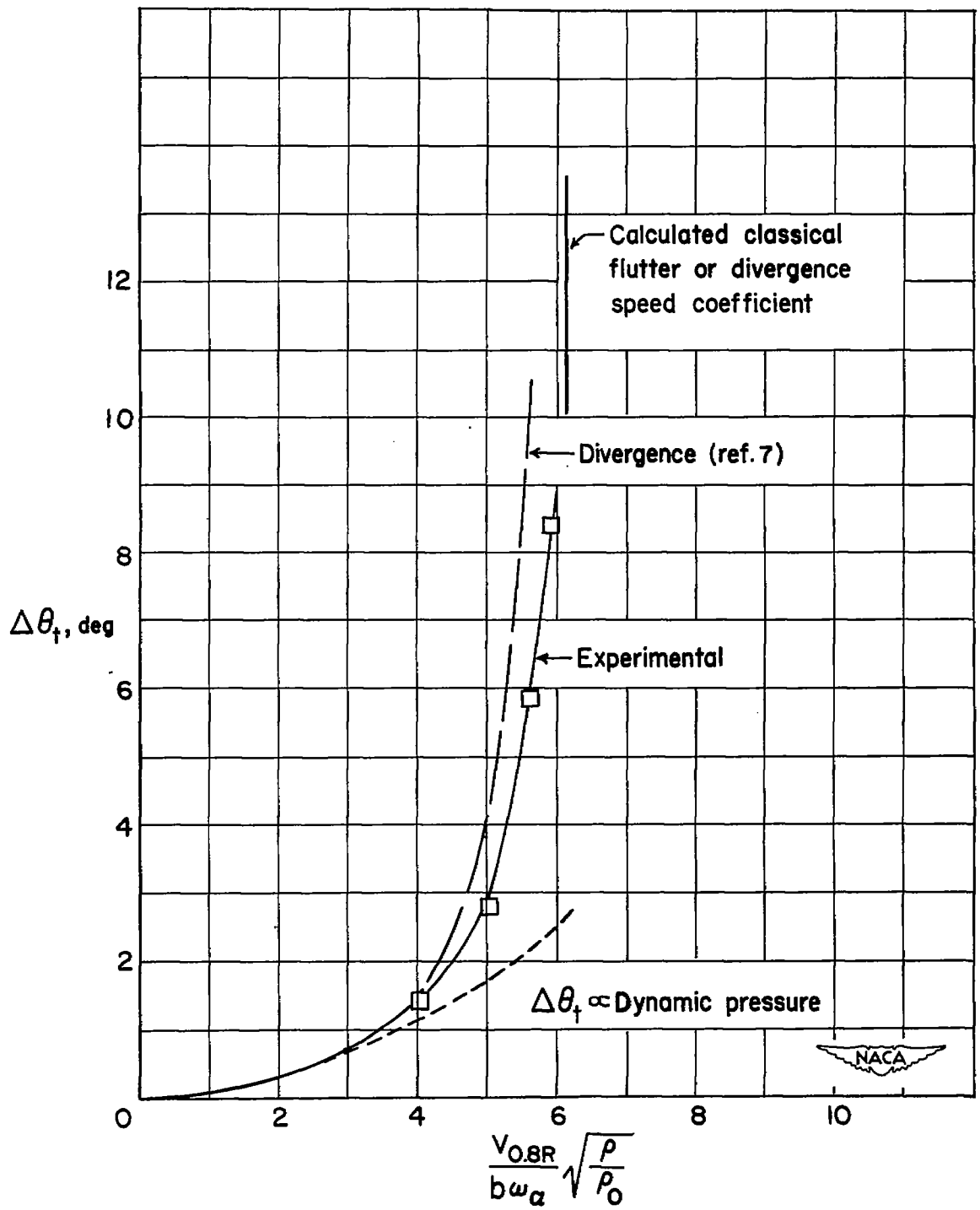

Figure 19.- A comparison between the experimental and calculated effect of the flutter speed coefficient on blade twist as the classical flutter or divergence speed is approached for blade 3(r). $(\theta_{0.8R})_s = 5^\circ$.

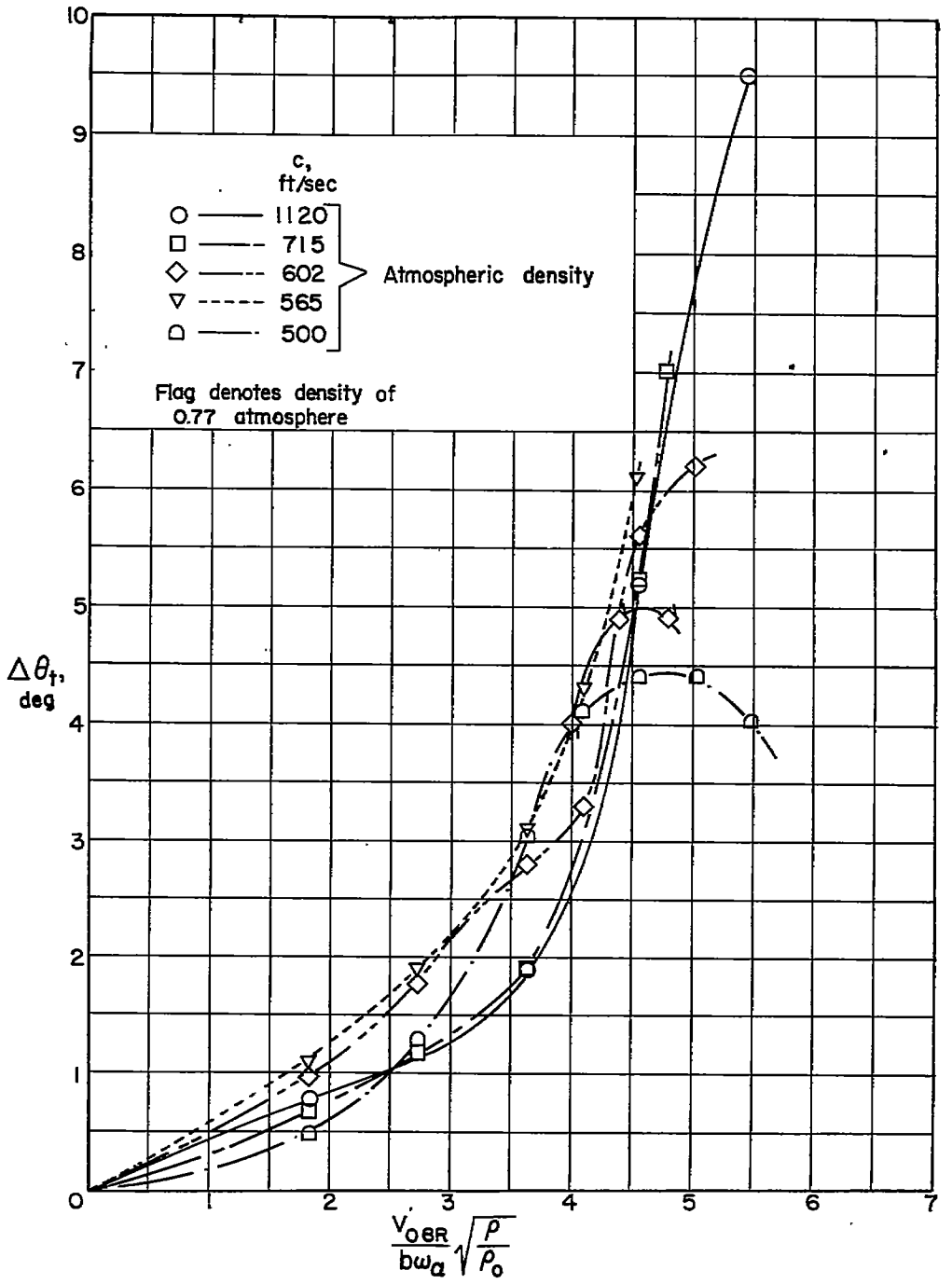

Figure 20.- The effect of the flutter speed coefficient on twist at the tip of blade 4(r) being rotated in mediums of different sound speeds. $(\theta_{0.8R})_s = 5°$.

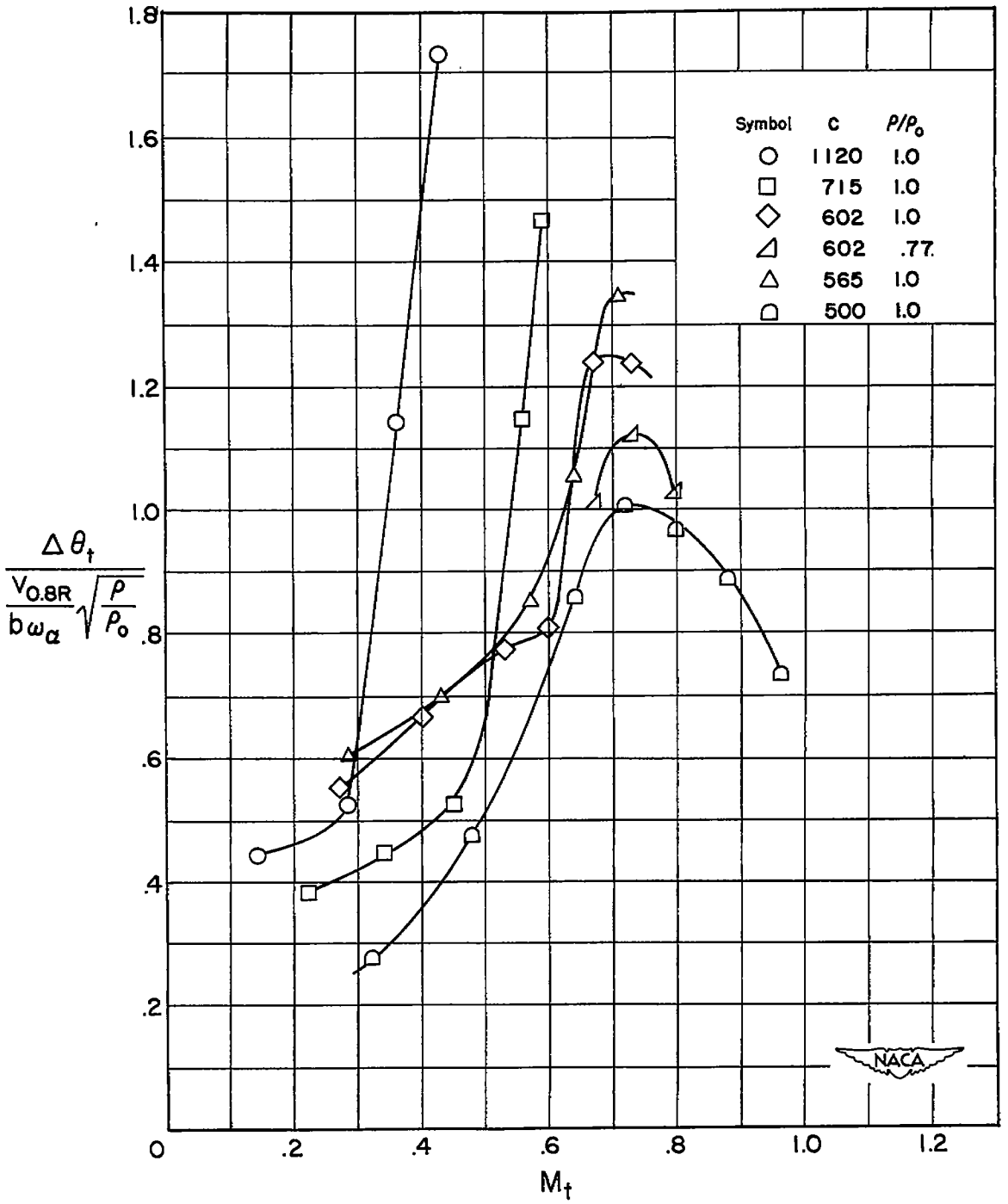

Figure 21.- The effect of blade divergence and Mach number on the measured twist at the tip of blade 4(r) being rotated in mediums at different sound speeds. $(\theta_{0.8R})_s = 5^\circ$.